

Fall 12-2016

## A Detailed Uncertainty Analysis of Heat Transfer Experiments Using Temperature Sensitive Paint

Anish Prasad  
*Embry-Riddle Aeronautical University*

Follow this and additional works at: <https://commons.erau.edu/edt>



Part of the [Aerospace Engineering Commons](#)

---

### Scholarly Commons Citation

Prasad, Anish, "A Detailed Uncertainty Analysis of Heat Transfer Experiments Using Temperature Sensitive Paint" (2016). *Doctoral Dissertations and Master's Theses*. 311.  
<https://commons.erau.edu/edt/311>

This Thesis - Open Access is brought to you for free and open access by Scholarly Commons. It has been accepted for inclusion in Doctoral Dissertations and Master's Theses by an authorized administrator of Scholarly Commons. For more information, please contact [commons@erau.edu](mailto:commons@erau.edu).

A DETAILED UNCERTAINTY ANALYSIS OF HEAT TRANSFER EXPERIMENTS  
USING TEMPERATURE SENSITIVE PAINT

A Thesis

Submitted to the Faculty

of

Embry-Riddle Aeronautical University

by

Anish Prasad

In Partial Fulfillment of the

Requirements for the Degree

of

Master of Science in Aerospace Engineering

December 2016

Embry-Riddle Aeronautical University

Daytona Beach, Florida

A DETAILED UNCERTAINTY ANALYSIS OF HEAT TRANSFER EXPERIMENTS  
USING TEMPERATURE SENSITIVE PAINT

by

Anish Prasad

A Thesis prepared under the direction of the candidate's committee chairman, Dr. Mark Ricklick, Department of Aerospace Engineering, and has been approved by the members of the thesis committee. It was submitted to the School of Graduate Studies and Research and was accepted in partial fulfillment of the requirements for the degree of Master of Science in Aerospace Engineering.

THESIS COMMITTEE



Chairman, Dr. Mark Ricklick



Member, Dr. Magdy Attia



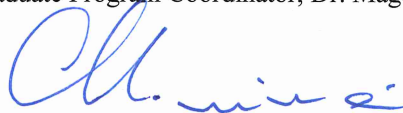
Member, Dr. Lakshmanan Narayanaswami



Graduate Program Coordinator, Dr. Magdy Attia

11.29.2016

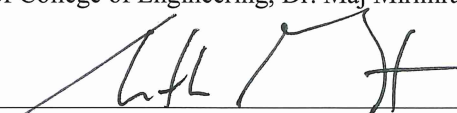
Date



Dean of College of Engineering, Dr. Maj Mirmirani

11/29/16

Date



Vice Chancellor, Academic Support, Dr. Christopher Grant

11/29/16

Date

## ACKNOWLEDGMENTS

First I would like to express my gratitude to my friends and family, especially to my parent's Prasad Ebenazer David and Sheba Dharni Rekha Jabin David, for their prayers and support. To my thesis advisor Dr. Mark Ricklick, I express my appreciation for all the support and guidance. Thank you for letting me be a part of the Propulsion Thermal Management Laboratory team or in other words the PTML family, you have been an awesome role model for all of us.

I would like to thank my thesis committee members, Dr. Magdy Attia and Dr. Lakshmanan Narayanaswami for their support and comments. I would also like to acknowledge my team mates, Yogesh Pai, Karthik Krishna, Royce Fernandes, Sundar Ramanathan, Christian Alexis Guzman Zurita, Angelo Andres Fonseca Pazmino, Yash T. Mehta, Bhushan Upalkar, Bianca A. De Angelo, Chase D Rossman, Neil P. Sullivan, Daniel M. Bystry Wells, Mayur D. Patel and everyone in the Gas Turbine Laboratory, for their support.

And finally the unspoken things that needs to be acknowledged: Volleyball, Badminton, Table Tennis, Swimming, Intramural, Starbucks, Thai ice tea, Gourmet Cuisine, Wine, Mazda RX-8, Beach, Springs, ISASI, NTSB, Steven F. Udvar-Hazy Center, Internet, Google, Wikipedia, Nikon D7000, Photoshop, WhatsApp, Home Depot, Walmart, Movies, TV Series, Anime, Manga, Nvidia, PC Games, Science and Bible; you have made my graduate career unforgettable.

## TABLE OF CONTENTS

LIST OF FIGURES .....	vi
LIST OF TABLES.....	viii
SYMBOLS.....	ix
ABBREVIATIONS .....	xi
ABSTRACT.....	xii
1. Introduction .....	1
1.1 Motivation.....	1
1.2 Thermodynamics.....	2
1.3 Turbine Blade Cooling.....	3
1.4 Pin Fin Channel .....	5
1.5 Rib Turbulated Channel.....	6
1.6 Temperature Sensitive Paint (TSP) .....	7
1.7 Need for Uncertainty .....	9
2. Introduction to Uncertainty .....	12
2.1 Errors in Measurement.....	12
2.2 Statistical Distribution .....	13
2.2.1 Normal Distribution.....	14
2.2.2 Student's t Distribution.....	15
2.3 Types of Uncertainty .....	17
2.3.1 Systematic Uncertainty.....	17
2.3.2 Random Uncertainty.....	18
2.3.3 Total Uncertainty .....	18
2.4 Root Sum Square Method (RSS).....	18
2.4.1 Single Measurement Uncertainty.....	19
2.4.2 Multiple Measurement Uncertainty.....	19
2.5 Level of Confidence in Uncertainty .....	20
2.6 Sensitivity.....	20
3. Literature Review .....	22
3.1 Uncertainty .....	22
3.2 Optimized Ribs .....	30
4. Problem Statement and Objective .....	32
5. Data Reduction.....	34
5.1 Introduction to Heat Transfer.....	34
5.1.1 Conduction Heat Transfer .....	34
5.1.2 Convection Heat Transfer .....	34
5.2 Uncertainty Data Reduction.....	36
5.2.1 Heat Leakage.....	37
5.2.2 Reynolds Number .....	38

5.2.3	Pressure Drop ( $\Delta P$ ) .....	38
6.	Experimental Model .....	39
6.1	Experimental Setup.....	39
6.2	TSP Setup.....	40
6.3	Intensity Validation.....	40
6.4	Rib Channel.....	41
6.4.1	Heat Leakage Test – Rib Channel .....	43
6.4.2	Smooth Channel Test – Rib Channel .....	44
6.5	Pin Fin Channel.....	45
6.5.1	Heat Leakage Test – Pin Fin Channel .....	45
6.5.2	Smooth Channel Test – Pin Fin Channel .....	46
7.	Uncertainty Analysis .....	47
7.1	Rib Channel.....	47
7.1.1	Student’s t Distribution (N=5) – Rib Channel .....	48
7.1.2	Student’s t Distribution (N=5) - Varying Heat Flux.....	54
7.2	Optimized Ribs .....	55
7.3	Pin-Fin Channel .....	57
7.3.1	Student’s t Distribution (N=5) – Pin Fin Channel .....	60
7.3.2	Effect of $\Delta T$ .....	64
7.3.3	Student’s t Distribution Vs Normal Distribution .....	65
7.3.4	Accuracy and Precision .....	67
7.4	Degradation of TSP .....	70
8.	Conclusion.....	72
	REFERENCES .....	74
	APPENDIX.....	77
A.	Data Reduction .....	77

## LIST OF FIGURES

Figure 1-1: Brayton Cycle .....	2
Figure 1-2: Turbine inlet temperatures over the years (Clifford, 1985) .....	4
Figure 1-3: Blade cooling techniques (Han, 2004).....	4
Figure 1-4: CFD simulation of flow features in a pin fin channel (Fernandes, 2016).....	6
Figure 1-5: Flow separation and reattachment around ribs (Han, 1985) .....	7
Figure 1-6: Jablonski diagram (Bell, 2001) .....	8
Figure 1-7: Reference Image & Data Image.....	9
Figure 2-1: Accuracy and Precision.....	12
Figure 2-2: Accuracy, Precision and Errors.....	13
Figure 2-3: Plots of normal PDF.....	15
Figure 2-4: Plots of student's t PDF .....	16
Figure 2-5: Comparison between student's t (N=5) and normal distribution.....	16
Figure 2-6: Comparison between student's t (N=30) and normal distribution.....	17
Figure 3-1: Estimating $\sigma$ from S (Robert J. Moffat, 1988).....	25
Figure 3-2: Uncertainty-Based Multidisciplinary Design Optimization (UMDO) (Yao et al., 2011) .....	28
Figure 3-3: Technical Approach (Tai and Mines, 2016) .....	29
Figure 3-4: Flow feature of rib 1 (Ranade et al., 2016) .....	30
Figure 3-5: Flow feature of rib 2 (Ranade et al., 2016) .....	31
Figure 3-6: Flow feature of rib 3 (Ranade et al., 2016) .....	31
Figure 4-1: First study of primary objective .....	32
Figure 5-1: Convection heat transfer from a plate (J.P. Holman).....	35
Figure 5-2: Variable Cascade for Nusselt Number.....	35
Figure 6-1: Schematic of wall setup .....	39
Figure 6-2: Schematic of experimental setup .....	39
Figure 6-3: TSP on a test piece.....	40
Figure 6-4: Intensity validation (Pai, 2016).....	41
Figure 6-5: Rib channel .....	42
Figure 6-6: Optimized ribs.....	42
Figure 6-7: Schematic of heat leak test.....	43
Figure 6-8: Heat leakage test - rib channel .....	43

Figure 6-9: Smooth channel test – rib (Upalkar, 2015) .....	44
Figure 6-10: Pin fin channel .....	45
Figure 6-11: Heat leak test – pin fin channel .....	46
Figure 6-12: Smooth channel test – pin fin (Fernandes, 2016).....	46
Figure 7-1: Temperature contour .....	47
Figure 7-2: Nu contour.....	47
Figure 7-3: Span-wise average Nu.....	48
Figure 7-4: Span-wise average Nu comparison .....	50
Figure 7-5 Uncertainty contribution in Nu .....	50
Figure 7-6: Uncertainty contribution in Nu, h, q .....	51
Figure 7-7: Uncertainty contribution in thermal conductivity.....	51
Figure 7-8: Temperature contribution to uncertainty.....	52
Figure 7-9: Nu comparison .....	56
Figure 7-10: Pressure drop comparison .....	57
Figure 7-11: Shunt resistor.....	58
Figure 7-12: Temperature contour – Pin fin .....	58
Figure 7-13: Nu contour – Pin fin.....	59
Figure 7-14: Span wise average Nu – Pin fin .....	59
Figure 7-15: Comparison of percentage of error .....	62
Figure 7-16: Span-wise average Nu comparison (pin fin).....	63
Figure 7-17: Comparison of current .....	63
Figure 7-18: Comparison of % error with respect to $\Delta T$ .....	65
Figure 7-19: Comparison of PDF.....	67
Figure 7-20: Accuracy and Precision.....	68
Figure 7-21: Accuracy and Precision - Corrected.....	69
Figure 7-22: Degradation of TSP.....	70



## LIST OF TABLES

Table 1-1: Uncertainty Example.....	10
Table 7-1: Measurements for Nu calculation.....	49
Table 7-2: Measurements for Re calculation and pressure drop ( $\Delta P$ ).....	53
Table 7-3: Measurement for Nu calculation (varying heat flux).....	54
Table 7-4: Measurements for Nu calculation (Pin fin).....	61
Table 7-5: Mean, min, max temperature measurements.....	61
Table 7-6: Uncertainty results.....	62
Table 7-7: Measurements for Nu calculation effect of $\Delta T$ .....	64
Table 7-8: Measurements for Nu calculation using different sample size.....	65
Table 7-9: Uncertainty results for different sample size.....	65
Table 7-10 Measurements for Nu calculation.....	66
Table 7-11 Uncertainty results.....	66

## SYMBOLS

$q''$	Heat flux	$W/m^2$
$\eta$	Efficiency	
$\Delta T$	Temperature Difference	K / °C
$D_h$	Hydraulic Diameter	M (meter)
$R$	Electrical Resistance	ohm ( $\Omega$ )
$h$	Heat transfer coefficient	$W/m^2K$
$I$	Current	A
$k$	Thermal Conductivity of Air	$W/mK$
$\dot{m}$	Mass flow rate	Kg/S
$Nu$	Nusselt Number	
$Re$	Reynolds Number	
$T$	Temperature	K or °C
$T_3$	Turbine Inlet Temperature	K or °C
$T_4$	Turbine Exhaust Temperature	K or °C
$T_w, T_s$	Temperature of the wall/surface	K or °C
$T_b, T_\infty$	Bulk temperature of the fluid	K or °C
$T_{inlet}$	Inlet fluid temperature	K or °C
$T_{outlet}$	Outlet fluid temperature	K or °C
$x$	Distance in Stream wise direction	m
$y$	Distance in Span wise direction	m
$x/D_h$	Stream wise distance in terms of hydraulic diameter	
$y/D_h$	Span wise distance in terms of hydraulic diameter	
$q$	Heat transfer rate	Watt (W)
$A, A_1, A_s$	Surface Area	$m^2$
$A_2, A_c$	Cross sectional area	$m^2$
$\rho$	Density of air	$Kg / m^3$

$\sigma$	Standard Deviation	The unit of the measurements
$N$	Number of samples	
$\vartheta$	Degree of freedom	
$v$	Velocity of air	m/S
$L^*$	Characteristic length	m
$\mu$	Dynamic viscosity	Ns / $m^2$
$t$	Thickness of the Inconel strip	m
$w$	Width of the Inconel strip	m
$L$	Length of the Inconel strip	m
$C_p$	Specific heat capacity	J/KgK
$\Delta P$	Pressure Drop	Pa (Pascal)
$P$	Pressure	Pa
$V$	Voltage	V (Volt)
$t_{95}$	Student t value with 95% confidence	
$e_1, e_2, e_n$	Bias errors	
$B_{\bar{x}}$	Systematic (Bias) uncertainty	
$b_{\bar{x}}$	Systematic (Bias) uncertainty divided by $t_{95}$	
$S_{\bar{x}}$	Random (Precision) uncertainty	
$u_{\bar{x}}$	Total uncertainty	
$U_{\bar{x}}$	Total uncertainty with 95% confidence	
$P/e$	Pitch to rib height ratio	
$e/D$	Ratio of rib height to hydraulic diameter	

## ABBREVIATIONS

CFD	Computational Fluid Dynamics
STAR-CCM+	Simulation of Turbulence in Arbitrary Regions-Computational Continuum Modeling
CMOS	Complementary Metal Oxide Semiconductor
TSP	Temperature Sensitive Paint
TBC	Thermal Barrier Coating
RSS	Root Sum Square
VARIAC	Variable Alternating Current Transformer
MATLAB	Matrix Laboratory

## ABSTRACT

Researcher: Anish Prasad  
Title: A Detailed Uncertainty Analysis of Heat Transfer Experiments using Temperature Sensitive Paint  
Institution: Embry-Riddle Aeronautical University  
Degree: Master of Science in Aerospace Engineering  
Year: 2016

Heat transfer experiments for different cooling techniques for a gas turbine blade are performed and the data are collected via temperature sensitive paint, ammeter, thermocouple and manometer measurement techniques. These data are subjected to uncertainty analysis and the major contributing parameter in the uncertainty is found. A tool to identify the major contributing parameter is devised to reduce the uncertainty in the experiment. Further the effect of temperature difference (surface temperature to bulk temperature) is studied to determine the impact on uncertainty and to determine its importance. The analysis between various implementations of the student's t distribution are conducted to determine the number of samples needed. This is important in experiments utilizing Temperature Sensitive Paint, where the measurement device is subject to degradation after extended use. A rib turbulated rig and a pin fin rig were used to conduct this research. It was found that the electrical current used to calculate the heat transfer coefficient is the major contributing parameter in the uncertainty. The increase in surface temperature reduced the percentage error from 9.5% to 5.6%. It was found that uncertainty calculated from student's t distribution with less number of samples gave about the same percentage error with less difference in comparison to the high number of samples.

## 1. Introduction

### 1.1 Motivation

In the gas turbine community, improving thermodynamic and propulsive efficiencies are today's major concern. Increasing the combustion temperature allows improvements in the engines fuel economy and power (Zuckerman & Lior, 2006). Limits in the turbine blade material operating temperature is an obstacle to these improvements. In order for the materials of the turbine blades to withstand the high temperatures cooling is required (Koff, 2004). The task of a cooling is not only to keep the maximum temperature of the blade itself below a safe level, but also minimize spatial variations in temperature that can create thermal stress (Iacovides, Launder, 2006). The efficiency of the gas turbine has since been steadily improving over the years by implementation of advanced cooling techniques and by the advancement in material technology.

Over the last few decades high performance materials have been used in making turbine blades. These sophisticated alloys have melting points below the combustion temperature of the engine. The combustion temperature ranges from 1300 °C to 1500 °C (Han et al., 2012), with a typical value of 1100 °C as the melting point of these materials. To avoid failure, the blades are cooled by the bleed air from the compressor section of the engine. The cooling must be carried out efficiently, in order to not impose efficiency penalties on the engine.

Much recent research has been concerned with the different cooling techniques implemented in the turbine blades. Various experiments are being conducted in regards to the development of cooling techniques. Experimental measurements always have uncertainty associated with them. Minimizing the uncertainty would increase the

usefulness of the data to designers, who must allow for this variability in the design process. If the uncertainty is not properly accounted for in design, it may cause unexpected change or fluctuation in system operation, or even function fault and failure in aerospace system (Yao et al., 2011).

## 1.2 Thermodynamics

The gas turbine works on the Brayton cycle, illustrated in the temperature – entropy diagram in Figure 1-1. The compressor section of the engine compresses the incoming air. Fuel is mixed and ignited with the compressed air in the combustor section. The combusted gases are then passed on to the turbine section, where the turbine blades extract energy from them.

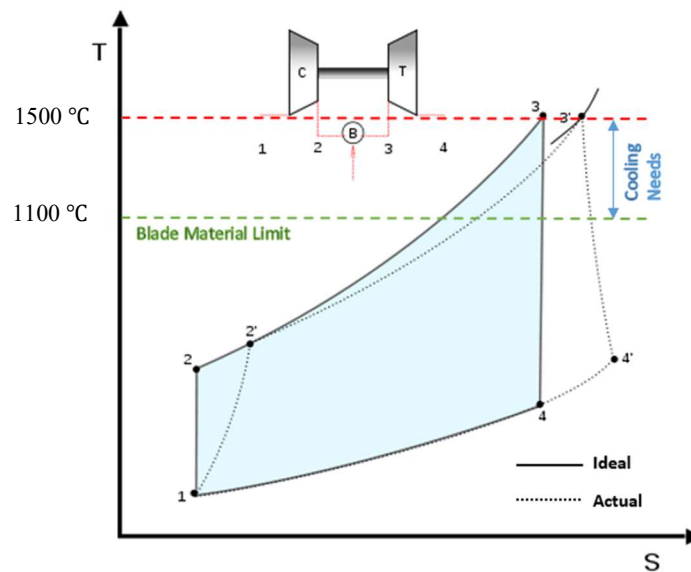


Figure 1-1: Brayton Cycle

The efficiency of the ideal Brayton cycle is governed by the equation,

$$\eta = 1 - \frac{T_4}{T_3} \quad (1)$$

In ideal case the Brayton cycle will not have any losses, but in the real world there are losses, which gives the actual Brayton cycle. Here  $T_3$  represents the turbine inlet temperature. As we can see higher the temperature at the inlet of the turbine, better the efficiency of the Brayton cycle. Hence gas turbine manufacturers strive to achieve the highest turbine inlet temperatures within the safe operating limits of the blade materials.

### **1.3 Turbine Blade Cooling**

The maximum attainable turbine inlet temperatures ultimately depend on the maximum combustion temperature of the fuels used for power generation today with some loss, which can reach temperatures close to 2000 K (taken from Figure 1-2). From Figure 1-2 its seen that the need for cooling started in late 1960's with the start of simple convection cooling (internal cooling). Later various methods such as film cooling, Thermal Barrier Coating (TBC) allowed to increase the operating temperature. The cooling of the blades a have advanced beyond simple smooth channel convection. (Downs and Landis, 2009).



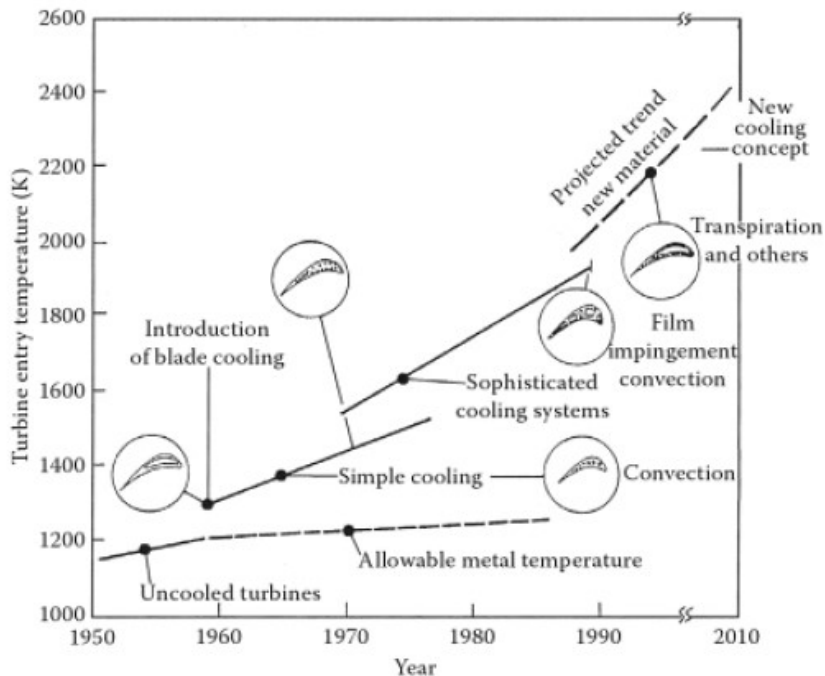


**Figure 1-2: Turbine inlet temperatures over the years (Clifford, 1985)**

Figure 1-3 shows the different cooling techniques implemented in a conventional gas turbine blade.

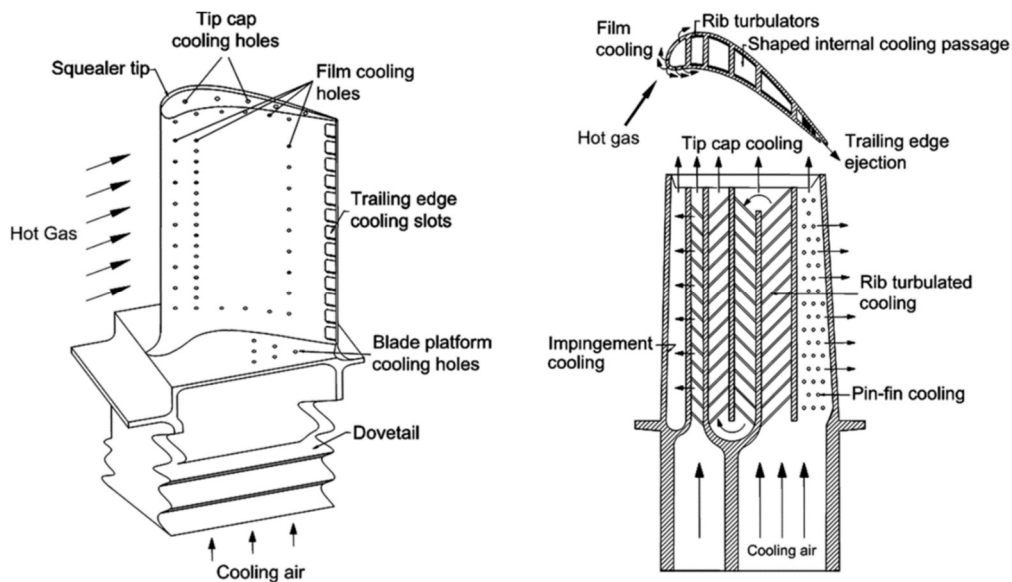


**Figure 1-3: Blade cooling techniques (Han, 2004)**

The cooling techniques for the turbine blade comprises of both internal and external cooling. The internal cooling technique comprises of three methods jet impingement channel, rib turbulated channel and pin fin channel. The bleed air from the compressor is passed through different internal channels. The impingement channel is located at the leading edge of the blade, the bleed air impinges on the hot surface of the blade, forming a stagnation region which enhances the heat transfer. The rib turbulated channels is located in the mid-section of the turbine blade, which creates recirculating flow zones which increase the heat transfer levels. The pin fin channel is located at the trailing edge of the blade. The internal surface area of the blade is increased by these pin fins thereby increasing the heat transfer. The pins also act as obstruction to the flow increasing the turbulence, further increasing heat transfer rates. The external cooling technique also uses bleed air from the compressor to form a film of cool air on the surface of the blades to protect it from the hot combustion gases.

#### **1.4 Pin Fin Channel**

A pin fin channel is made up of fins, usually cylindrical, arranged in an array. Figure 1-4 represent the flow feature in a typical pin fin channel geometry with instantaneous velocity. An internal cooling channel with a pin fin array is characterized by regions of accelerated flows between the pins, stagnation flows, localized low and high pressure regions, flow separation zones and end wall boundary layer flow features that enhance the rates of convective heat transfer (Ames (2006), Chyu (1999), Metzger (1982)). The resulting shedding of vortex caused by unsteady separation is a significant driver of heat transfer on the backside of the pin (Ames & Dvorak, 2006). The main contributors to the

heat transfer are the stagnation at the leading edge and the horseshoe vortex created at the trailing edge of the pin (Chyu et al., 1999).

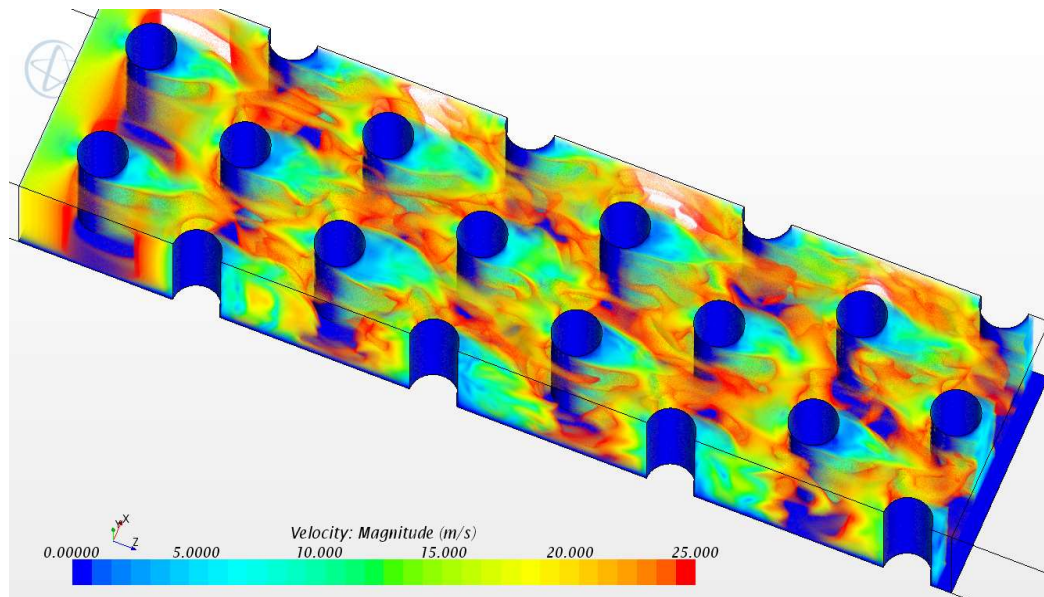


**Figure 1-4: CFD simulation of flow features in a pin fin channel (Fernandes, 2016)**

## 1.5 Rib Turbulated Channel

Ribs are protrusions or extended surfaces placed on the target wall of the flow channel. Various configurations of rib placement and angle are possible with significant effect on heat transfer and pressure drop. From previous studies the rib pitch to height ratio ( $P/e$ ), the rib height to hydraulic diameter ( $e/D$ ) and rib angle of attack are the main factors affecting the heat transfer coefficients and friction factors (Han, 1985).

From Figure 1-5 it is seen that the rib obstructs the flow thereby detaching the oncoming flow, the flow trips and it separates on top of the rib then it reattaches to the wall between the ribs. The boundary layer at the end wall is disturbed by this flow separation and reattachment, which increases the heat transfer. The fact that it only disturbs the flow

near the wall, the overall heat transfer is enhanced with relatively low pressure drop (Zuckerman, 2005).

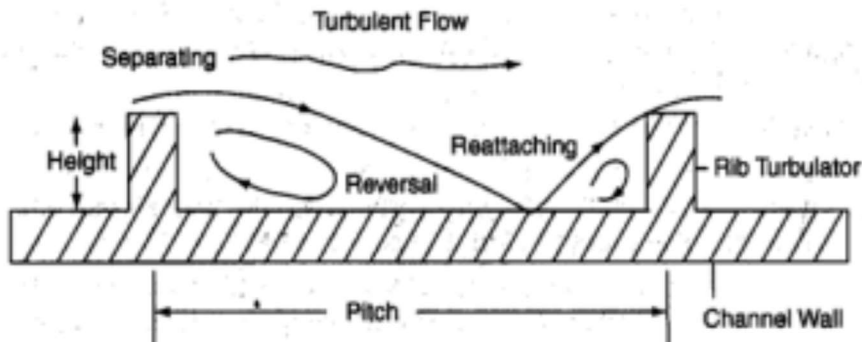


**Figure 1-5: Flow separation and reattachment around ribs (Han, 1985)**

Rib spacing has a significant effect on the performance of the channel. Hence optimization is a key aspect in order to obtain optimal results for heat transfer and pressure loss.

## 1.6 Temperature Sensitive Paint (TSP)

TSP provides a convenient way to obtain temperature data. It is a luminescent paint with fluorescent molecules suspended within a binder. The TSP molecules are excited to a higher energy state when exposed to light of appropriate wavelength (excitation wavelength). Jablonski diagram shown in Figure 1-6 describes the transition of the molecules. They can return to ground state by emitting photons of particular wavelength (emission wavelength) through luminescence or by thermal quenching without emitting photons. In thermal quenching the molecules vibrate and collide with one another, losses energy and returns to ground state. For this research ISSI brand UniCoat TSP was used having excitation wavelength of 380 – 520 nm and emission wavelength of 500 – 720 nm. An ultraviolet light with a wavelength of 460 nm (from manufacturer ISSI) was used to

excite the TSP molecules. The intensity of the paint varies with the amount of photons emitted. Increase in temperature will statistically increase the return of photons to ground state through thermal quenching, thereby decreasing the intensity of the paint (intensity is related to the measure of photons emitted from the TSP, which are then captured by the CMOS sensor in a scientific grade camera).

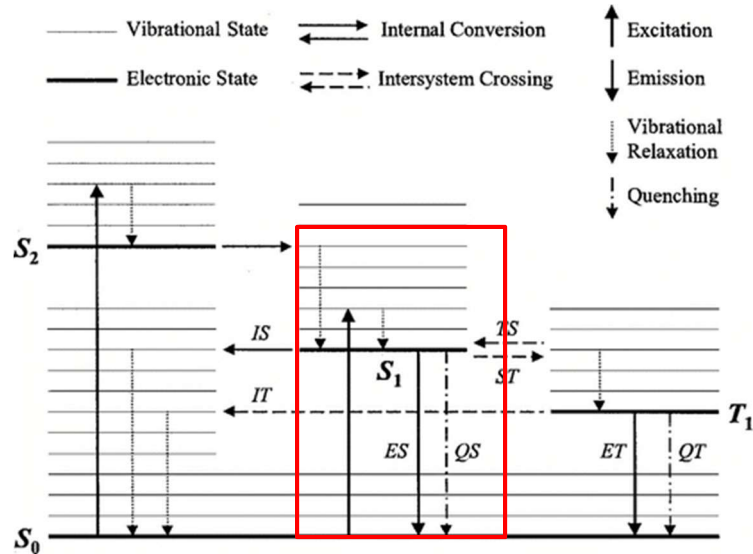


**Figure 1-6: Jablonski diagram (Bell, 2001)**

In Figure 1-7, the reference image is taken before the experiment with known intensity and reference temperature (measured with a thermocouple on the surface, and ensured it is uniform by cross referencing to the other thermocouple on different location on the surface). The data image, where the intensity of the paint is known but the surface temperature of the paint is unknown.

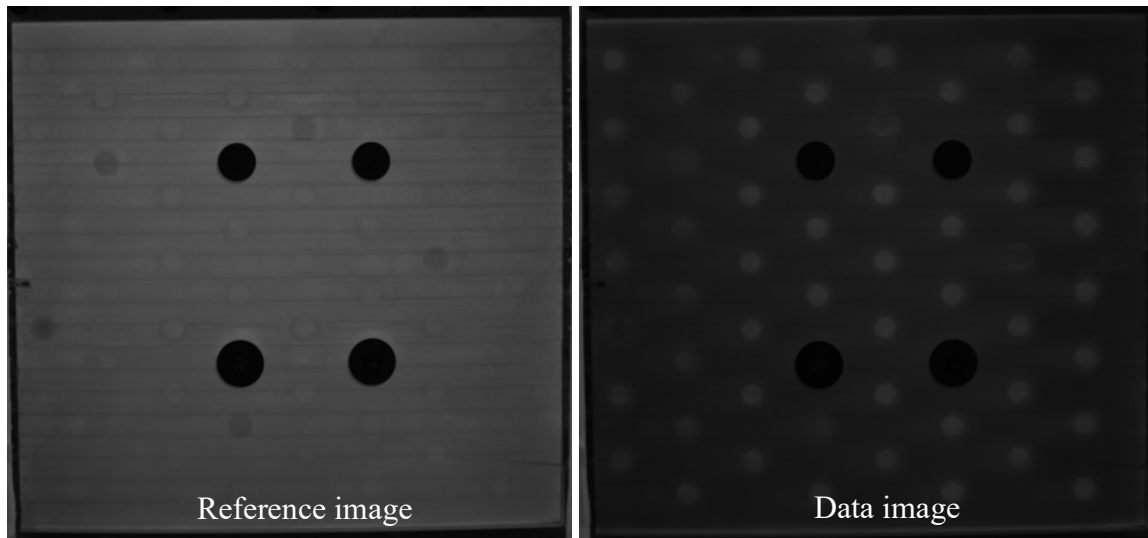


**Figure 1-7: Reference Image & Data Image**

TSP is calibrated with a calibration curve of intensity ratio vs temperature difference and used in calculating the unknown surface temperature of the data image. The calibration uncertainty of TSP was found to be  $\pm 0.93$  °C for temperature ranges of 22 to 90 °C in previous studies (Liu, 2006). A scientific grade camera (CMOS) is used to capture the intensity of the light emitted by the TSP, with a long pass filter (wavelength 550 nm) to distinguish between the excited wavelength and the emitted wavelength. A detailed analysis and description of TSP and PSP technologies has been presented by Liu (2006), Sullivan (1995).

### **1.7 Need for Uncertainty**

The error in the result or measurement is usually defined as the difference between the true value and the calculated or measured value. This is only possible in cases where the true value is known from a baseline result or from analytical solutions. Therefore, in all other cases we cannot confidently state what the error might be. Hence the concept of uncertainty is introduced, which is used to refer to a possible value that the error may have

(Moffat, 1988). But the uncertainty or what one may assume the error might be, may vary considerably depending upon the particular circumstances of the observation of the variables, which means the basic quantity observed directly in the experiment as opposed to the results, which is obtained by calculations with the recorded values of the variables (Kline & McClintock, 1953). The values of the variables are called data, in some cases the result will be the same as the data (for single measurement). The propagation of uncertainty means, the way in which the uncertainties in the variable will affect the uncertainty in the results.

To illustrate with an example, take heat transfer coefficient ( $h$ ), which is calculated by the formula,

$$h = \frac{q''}{\Delta T} \quad (2)$$

where  $\Delta T$  is the driving temperature difference, typically taken as the difference between the surface and bulk temperature.  $\Delta T$ ,  $q''$  are the variables used to calculate the result  $h$ .

**Table 1-1: Uncertainty Example**

	$q''$ ( $W/m^2$ )	$T_s$ ( $^{\circ}C$ )	$T_b$ ( $^{\circ}C$ )	$\Delta T$ ( $^{\circ}C$ )	$h$ ( $W/m^2K$ )
Measured value	1000	40	20	20	50
True value	1000	39	21	18	55.5

In Table 1-1 the measured value and the true values are given. It is assumed that the measured value for surface temperature ( $T_s$ ) and the bulk temperature ( $T_b$ ) are different from their true values due to the thermocouple error of  $\pm 1^{\circ}C$  (from manufacturer omega).

Heat flux ( $q''$ ) is assumed to be correct for this example. In reality all the measured values contain some amount of error.

From table 1-1, the error between the calculated and the true value is 10%. When the calculated value is presented, the quality of the value is determined by the range of the uncertainty given. The value of  $h$  in this example should be given its uncertainty of  $50 + 5.5 \text{ W/m}^2\text{K}$  when presenting the obtained result.

The overall purpose of this research is to investigate the uncertainty of heat transfer experiments in Embry Riddle Aeronautical University.



## 2. Introduction to Uncertainty

Uncertainty is the possible value that the error may have (Moffat, 1988). It is calculated using either single sample or multiple sample uncertainty method. The latter which is used in this research has its calculation based on two errors, systematic (bias) and precision error.

### 2.1 Errors in Measurement

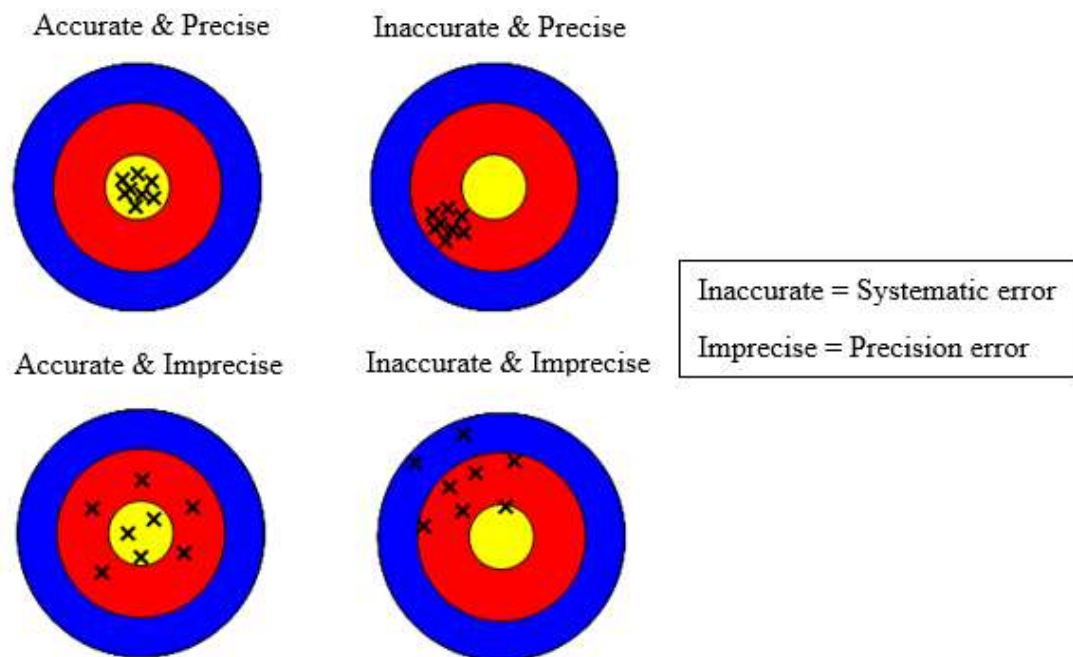


**Figure 2-1: Accuracy and Precision**

Figure 2-1, clearly explains the difference between the accuracy and precision of measurements. In regards to accuracy and precision, each term has its own unique error. The systematic error or in other terms called as the bias error, which is given from the measuring device. Each measuring device has information for the accuracy of the measurements taken, which is incorporated for the bias error of that measuring device. The precision error or in other terms called as the reproducibility or random error is from the

set of readings taken. It is to see whether the measurements are repeatable. It is calculated from the standard deviation of the set of measurements taken.

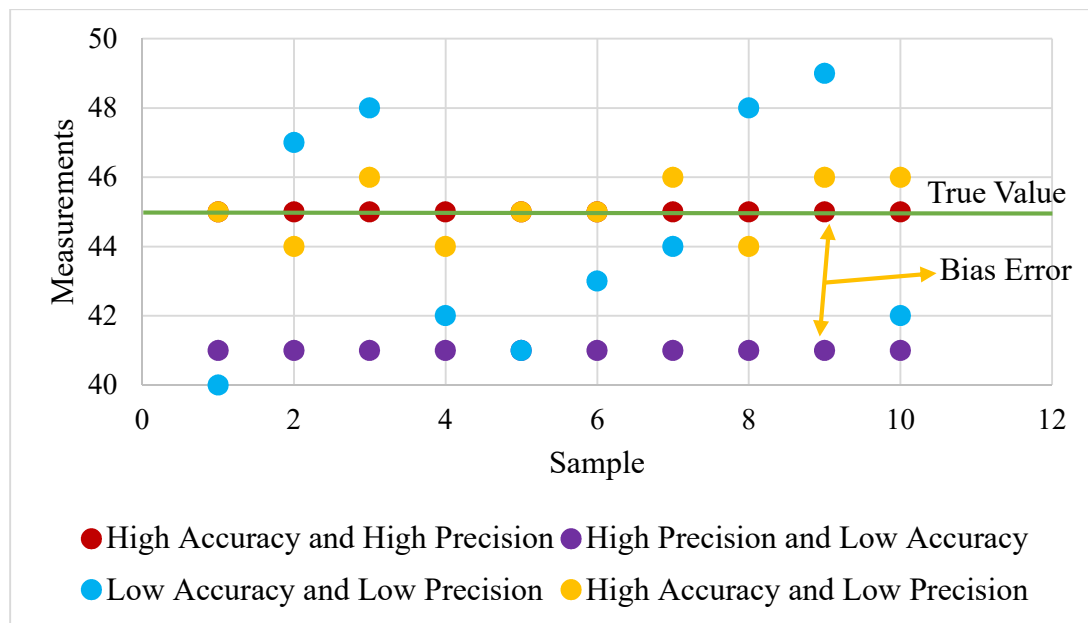


**Figure 2-2: Accuracy, Precision and Errors**

Figure 2-2, explains the errors, accuracy and precision in technical aspects. The values which give of high precision and less accuracy is due to the bias error of the measuring device. And the one which gives of high accuracy and less precision is due to the repeatability of the experiment and gives to precision error.

## 2.2 Statistical Distribution

Random variables are encountered in everyday life, such as strength of a material, life of a spark plug, turbulence intensity and so on. They have come to play a major role in engineering. Random variables are measured and analyzed in terms of their statistical and probabilistic properties, an underlying feature of which is the distribution function (Catherine Forbes, Merran Evans, Nicholas Hastings, Brian Peacock, 2011). Although there are various potential distribution models, in practice only a relatively small number

of distribution models are used. The probability density function (PDF) is used to distinguish each distribution having its own standard deviation with given degrees of freedom. It determines the probability that the random variable assumes a value under the bell curve.

### 2.2.1 Normal Distribution

The scatter of the measured data set will be distributed symmetrically around a central tendency (the mean of the scatter). This forms a bell curve. Random scatter in engineering measurements are normally distributed.

The normal distribution describes a family of continuous probability distributions having the same general shape and differing in their location (that is, the mean or average) and scale parameters (that is, the standard deviation) (Mohammad Ahsanullah, Golam Kibria, Mohammad Shakil, 2014). The shape of the probability density function of the normal distribution is a symmetrical bell shaped curve as shown in Figure 2-3.

A set of random variables  $x$  will have a normal distribution governed by the PDF,

$$f_x(x) = \frac{1}{\sigma\sqrt{2\pi}} e^{-\frac{(x-\mu)^2}{2\sigma^2}}, \quad -\infty < x < \infty \quad (3)$$

Where  $\mu$  is the mean and  $\sigma$  is the standard distribution. When the mean is 0 and the standard deviation is 1 then the distribution is called standard normal distribution.

And the PDF will become,

$$f_x(x) = \frac{1}{\sigma\sqrt{2\pi}} e^{-\frac{x^2}{2}}, \quad -\infty < x < \infty \quad (4)$$

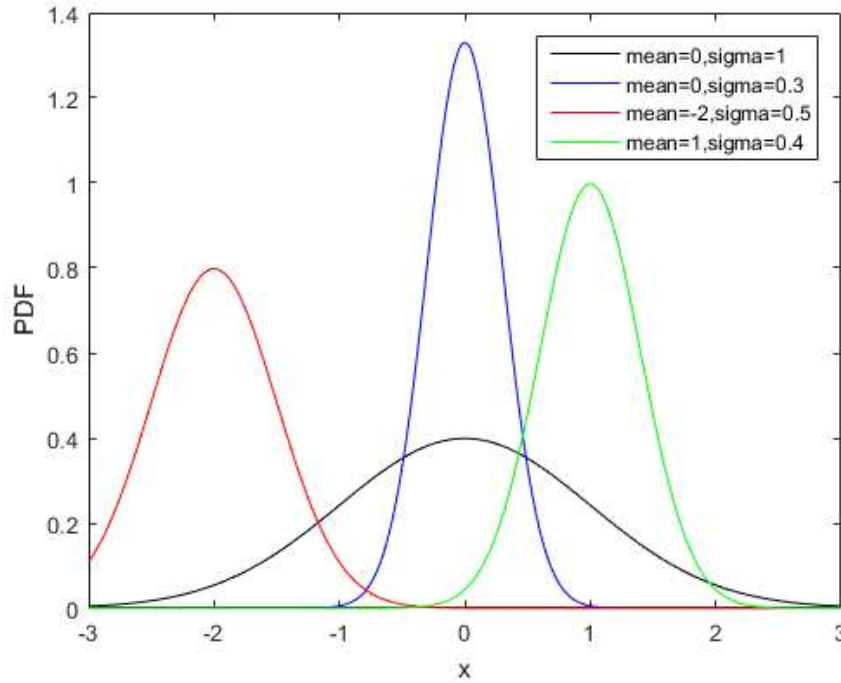


**Figure 2-3: Plots of normal PDF**

### 2.2.2 Student's t Distribution

Student's t distribution is the simplification of normal distribution. It also defines the family of continuous probability distributions (Mohammad Ahsanullah, Golam Kibria, Mohammad Shakil, 2014). The PDF is given by,

$$f_{t,\vartheta}(x) = \frac{1}{\sqrt{\vartheta B\left(\frac{\vartheta+1}{2}, \frac{\vartheta}{2}\right)}} \left(1 + \frac{x^2}{\vartheta}\right)^{-\frac{\vartheta+1}{2}} \quad -\infty < x < \infty \quad (5)$$

Where B is the beta function and  $\vartheta$  is the degree of freedom (N-1). From Figure 2-4, it is seen that the shape of the bell curve changes with changes in the degree of freedom ( $\vartheta$ ), the tail is thicker on the ends for less degree of freedom and thinner on the ends for higher degree of freedom. Student t distribution approaches the standard normal distribution when sample size  $N \rightarrow \infty$ .

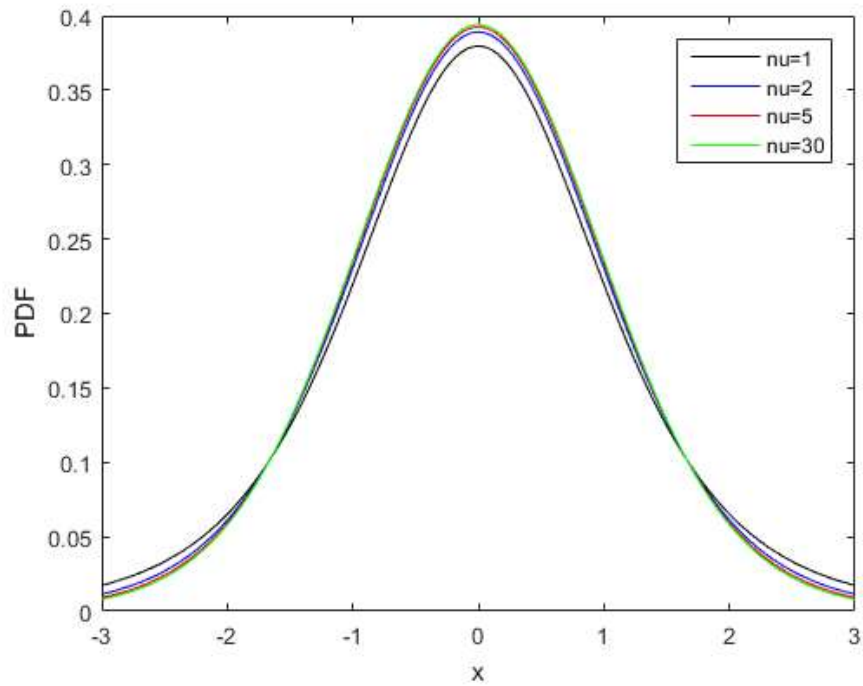


**Figure 2-4: Plots of student's t PDF**

From Figure 2-5 and 2-6 it is clearly seen that for a sample size of 30 the student's t distribution reaches the normal distribution, needless of  $N \rightarrow \infty$ .

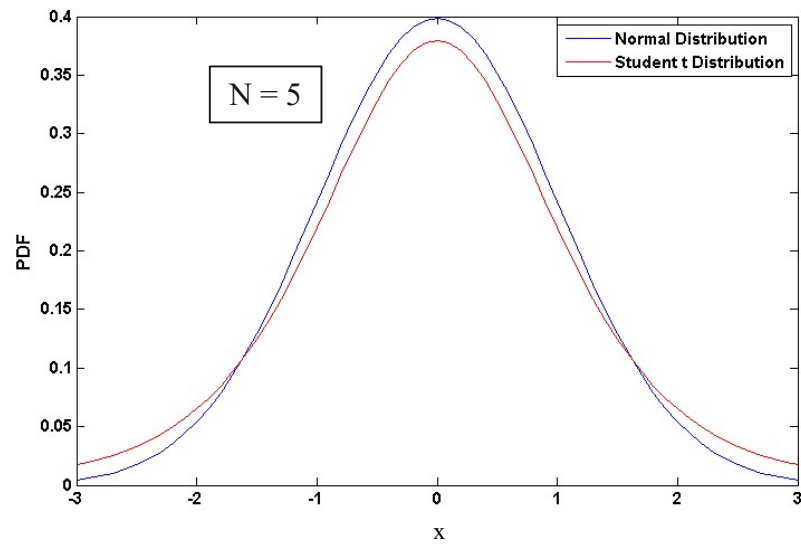


**Figure 2-5: Comparison between student's t (N=5) and normal distribution**

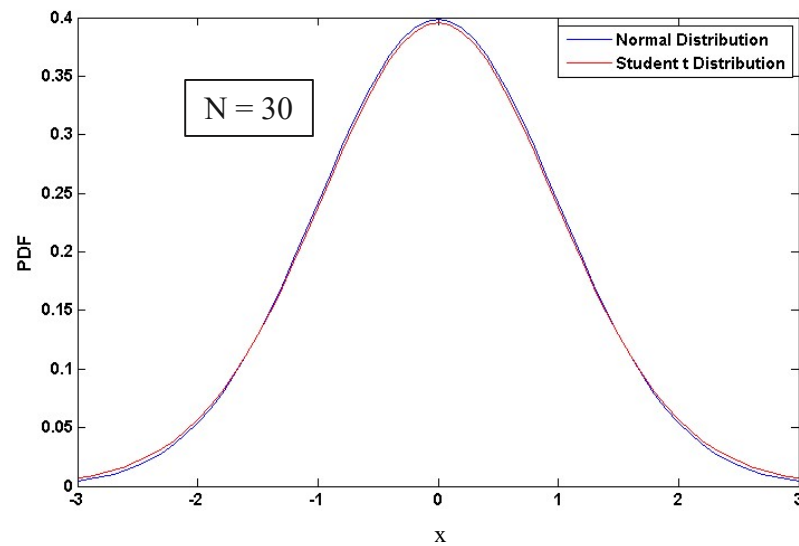


**Figure 2-6: Comparison between student's t (N=30) and normal distribution**

## 2.3 Types of Uncertainty

Uncertainty is divided into two types systematic and random uncertainty, calculated from systematic and random error. Both contribute to calculate the total uncertainty.

### 2.3.1 Systematic Uncertainty

Systematic uncertainty is calculated from the bias error of the measurements made from a measuring device. It remains the same for a single test. It uses the root sum square method to capture the errors in the measurement. It is given by the relation,

$$B_{\bar{x}} = \sqrt{e_1^2 + e_2^2 \dots \dots + e_n^2} \quad (6)$$

In this relation the variables  $e_1, e_2, \dots, e_n$  are the different types of errors in a measuring device for a single measurement. In some places it is also termed as bias uncertainty.

### 2.3.2 Random Uncertainty

The precision error from the repeatability of the experiment gives rise to random uncertainty or precision uncertainty. Its calculated from the standard deviation and also called as the standard deviation of the mean.

$$S_{\bar{x}} = \frac{\sigma_x}{\sqrt{N}} \quad (7)$$

Where  $\sigma_x$  is the standard deviation of the recorded measurement and N is the number of recorded measurement, in other words sample size.

### 2.3.3 Total Uncertainty

It's the combination of systematic and random uncertainty, with the utilization of root sum square method.

$$u_{\bar{x}} = \sqrt{B_{\bar{x}}^2 + S_{\bar{x}}^2} \quad (8)$$

## 2.4 Root Sum Square Method (RSS)

Describing about calculating uncertainty, papers from Kline & McClintock (1953), Moffat (1988), ASME PTC 19.1 (2005) all talk about the usage of root sum square method (RSS). The determination of an uncertainty at some level of confidence is based on the root-sum-square of the systematic and random standard uncertainties multiplied times the appropriate expansion factor for the desired level of confidence (usually “2” for 95%) (ASME PTC 19.1, 2005). The multiplication factor 2 is obtained from t table for degree of freedom greater than 30.

### 2.4.1 Single Measurement Uncertainty

The RSS method is utilized to calculate the uncertainty of a single measurement. For measurements  $x_1, x_2, \dots, x_n$  the uncertainty is calculated to be,

$$u_{\bar{x}} = \sqrt{B_{\bar{x}}^2 + \bar{S}_{\bar{x}}^2} \quad (9)$$

Where  $B_{\bar{x}}$  and  $\bar{S}_{\bar{x}}$  are the systematic and random uncertainty for the measurements. Single sample uncertainty is less complicated since the error is from one measuring device and from one set type of measurements.

### 2.4.2 Multiple Measurement Uncertainty

Multiple measurements uncertainty lacks the simplicity in comparison the single measurement uncertainty. When two different type of measurements are recorded from two different type of measuring device each having its own systematic and random uncertainty, then the error of those respective measurements needs to be properly propagated to get the final uncertainty value. Therefore, it requires a first order derivative in the root sum square method to give sensitivity to that measurement variable. Let's say that  $y$  is a variable calculated by two measured variable  $m$  and  $x$ ,

$$y = mx \quad (10)$$

Then the propagation of error by using root sum square method will be,

$$u_y = \sqrt{\left(\frac{\partial y}{\partial m} * B_m\right)^2 + \left(\frac{\partial y}{\partial x} * B_x\right)^2 + \left(\frac{\partial y}{\partial m} * \bar{S}_m\right)^2 + \left(\frac{\partial y}{\partial x} * \bar{S}_x\right)^2} \quad (11)$$

The calculated uncertainty  $u_y$  take into consideration the errors of each measurements by propagating the error throughout using RSS.



## 2.5 Level of Confidence in Uncertainty

The confidence level states that the probability of a parameter's value falls within a certain specified range of values. The Student's  $t$  is chosen on the basis of the level of confidence desired and the degrees of freedom (ASME PTC 19.1, 2005). Usually for a large degree of freedom the  $t$  value is taken to be 2 (approx. 1.96) and multiplied with the calculated uncertainty to give the confidence to that uncertainty value. From  $t$  tables it can be noted that for a degree of freedom (sample size – 1) greater than 1000 the  $t$  value will be approx. 1.96. The final uncertainty with the level of confidence is given by,

$$U_{\bar{x}} = t_{95} * u_{\bar{x}} \quad (12)$$

The  $t$  value chosen varies by the level of confidence desired and the degree of freedom considered. The  $t_{95}$  value should only be affected by the random uncertainty but not the systematic uncertainty, hence the systematic uncertainty is divided by the  $t_{95}$  value, before taken into root sum square to calculate the total uncertainty.

$$b_{\bar{x}} = \frac{B_{\bar{x}}}{t_{95}} \quad (13)$$

$$u_{\bar{x}} = \sqrt{b_{\bar{x}}^2 + S_{\bar{x}}^2} \quad (14)$$

## 2.6 Sensitivity

The differentiation term used in the calculating the multiple measurement uncertainty is called as the sensitivity coefficient or contributing factors to the uncertainty.

Consider the same relation with  $x$ ,  $y$ ,  $m$  variables,

$$1 = \frac{\left(\frac{\partial y}{\partial m} * B_m\right)^2 + \left(\frac{\partial y}{\partial x} * B_x\right)^2 + \left(\frac{\partial y}{\partial m} * \bar{S}_m\right)^2 + \left(\frac{\partial y}{\partial x} * \bar{S}_x\right)^2}{u_y^2} \quad (15)$$

The differential term  $\frac{dy}{dm}$  is called as the sensitivity coefficient or the contributing factor for the variable  $B_m$  in the total uncertainty calculated. To get the corresponding contributing percentage of each variable to the uncertainty, the related term for example  $\left(\frac{dy}{dm} * B_m\right)^2$  is divided by  $u_y^2$  and multiplied by 100. This gives the contributing percentage of systematic uncertainty of the variable m in regards to the total uncertainty.

These are the required steps for analysis of uncertainty using multiple sample uncertainty method. The selection of RSS method and the difference between single sample and multiple sample uncertainty are discussed briefly in the literature.

### 3. Literature Review

#### 3.1 Uncertainty

According to ASME PTC 19.1 (2005) the objective of analysis of uncertainty is to facilitate communication regarding measurement and test results, identify potential sources of error, permit rational selection of instruments, facilitate the design of cost-effective tests, advise if the test is feasible and induce a level of confidence in the test results. The ASME PTC 19.1 is a handbook for uncertainty giving out the proper steps in calculating the uncertainty in the final result. The steps mentioned have been explained in detail in Chapter 2, Introduction to Uncertainty.

Kline & McClintock (1953), described about uncertainties in single sample experiments. Single sample uncertainty analysis is based on a single measurement, is done in design phase of an experiments, for selection of effective measurement systems and methodologies for measurement. The authors have analyzed the calculation of uncertainty using three theorems and correlated three relations.

If R is the result, let it be a function of 'n' independent variables,  $v_1, v_2, v_3,$

$$R = R(v_1, v_2, \dots \dots v_n) \quad (16)$$

$$w_R = \left| \frac{\partial R}{\partial v_1} w_1 \right| + \left| \frac{\partial R}{\partial v_2} w_2 \right| + \dots \dots \dots \left| \frac{\partial R}{\partial v_n} w_n \right| \quad (17)$$

The first theorem gave this relation, where 'w' is the uncertainty interval. This relation is referred as the linear equation.

The correlation based on second theorem was used to calculate the standard deviation of R, the relation is given by,

$$\sigma_R = \left[ \left( \frac{\partial R}{\partial v_1} \right)^2 \sigma_1^2 + \left( \frac{\partial R}{\partial v_2} \right)^2 \sigma_2^2 + \dots \dots \dots \left( \frac{\partial R}{\partial v_n} \right)^2 \sigma_n^2 \right]^{1/2} \quad (18)$$

According to third theorem, the relation was correlated to get the uncertainty interval for the result, when the variables are normally distributed.

$$w_R = \left[ \left( \frac{\partial R}{\partial v_1} w_1 \right)^2 + \left( \frac{\partial R}{\partial v_2} w_2 \right)^2 + \dots \dots \dots \left( \frac{\partial R}{\partial v_n} w_n \right)^2 \right]^{1/2} \quad (19)$$

This equation is referred as the second power equation and it is directly used as an approximation for calculating the uncertainty intervals in the result.

The linear and the second power equations are compared using different distributions to find out which is superior.

For the result which is proportional to the sum of two variables, it is found that, the second power equation predicts the uncertainty interval for the result within 10 % of the correct value but the linear equation predicts the uncertainty interval varying from the correct value by 40 % (Kline & McClintock, 1953). And for result which is to be the sum of infinite variables, it is clearly found that the second power equation is superior to the linear equation. As the error in the interval of the second power equation is no more than 15% but for the linear equation it becomes infinite.

Hence it is entirely reasonable to use the second power equation in calculating the uncertainty interval for the result. It applies for both single sample and multiple sample uncertainty. The second power equation is a useful tool in selection of instrumentation for the experiments. This second power equation is also termed as RSS (Root Sum Square) in different literatures.

Moffat (1988), he described in detail about the uncertainties in experimental results for both single and multiple samples. The term uncertainty interval and uncertainty are

used interchangeably. The single sample uncertainty generates three descriptors for each result, zeroth, first and nth order uncertainty estimates (Moffat,1988). Each estimate will have its own total uncertainty. The zeroth order uncertainty interval estimates the overall uncertainty (fixed and variable errors) arising from the instrumentation itself. The first order uncertainty interval estimates the scatter in the result of repeated trials using the same equipment, procedures and instrumentation each time but with the process running. The Nth order uncertainty interval estimates the overall uncertainty in the experiment, it also includes the effects of process unsteadiness. It acknowledges the fixed and variable errors in the measuring system and in all the corrections applied to the observed value.

The fixed (bias) errors are obtained from the components used. The overall fixed error is the RSS combination of the component errors, which is evaluated the same way for single and multiple sample uncertainty. Variable errors are different for single and multiple sample uncertainty. For a single sample experiment the variable error arises from the fact that each observation is made only once, whereas in multiple sample experiments the variable error in a set of measurements can be determined from the variance (square of standard deviation) of the set itself. Therefore, for a single sample experiment an ancillary experiment is required to estimate the variable component of uncertainty. The second difference is that the uncertainty intervals should be referred to an individual measurement, not the mean of the set. This means the standard deviation of the population should be used for single sample uncertainty, not the standard deviation of the mean of the set, which is used for multiple sample uncertainty.

The difficulty over here is to find the standard deviation of the population. Hence a chi-squared test is utilized to give a relation between the sample ( $s$ ) and population ( $\sigma$ )

standard deviation with regards to the number of samples ( $n$ ), as described in Figure 3.1.

$n$	$\sigma/S$ (maximum)	$\sigma/S$ (minimum)
1	31.62	0.45
2	6.26	0.52
5	2.45	0.63
10	1.75	0.70
20	1.44	0.76
30	1.34	0.80
40	1.28	0.82
50	1.24	0.84
60	1.22	0.85

**Figure 3-1: Estimating  $\sigma$  from  $S$  (Robert J. Moffat, 1988)**

From Figure 3-1, for a given sample size the standard deviation of the population will lie between the maximum and minimum value. And its selection depends on the user, whether to have a largest or the smallest random uncertainty estimate of the measuring component.

The zeroth order uncertainty of a measurement is the RSS of fixed and random uncertainty components introduced by the measuring systems. This is given by the relation,

$$\delta X_{i,0} = \left[ (\delta X_{i,fixed})^2 + (2\sigma_{i,0})^2 \right]^{1/2} \quad (20)$$

Where  $\delta X_{i,fixed}$  is the overall fixed error uncertainty of the measuring system and  $\sigma_{i,0}$  is the standard deviation of the population of individual measurements from the measuring system when its input is stationary.  $\delta X_{i,0}$  corresponds to the uncertainty with 95% confidence.

The first order uncertainty interval for each measurement type must be measured in an auxiliary experiment. It describes the scatter that would be expected in a set of observations using the given apparatus and instrumentation system, while the observed process is running. The first order uncertainty includes variable error and process unsteadiness. It does not include the fixed errors. It is denoted by  $\delta X_{i,1}$ .

The Nth order uncertainty is the RSS of first order uncertainty with the RSS of fixed errors from every source. It is given by the relation,

$$\delta X_{i,N} = \left[ (RSS \delta X_{i,fixed})^2 + (\delta X_{i,1})^2 \right]^{1/2} \quad (21)$$

For describing the uncertainty in the final result, if result R of the experiment is calculated from the set of measurements given by,

$$R = R(X_1, X_2, X_3, \dots, \dots, X_n) \quad (22)$$

Then the relation for the uncertainty in the result is given by,

$$\delta R_X = \left[ \left( \frac{\partial R}{\partial X_1} \delta X_1 \right)^2 + \left( \frac{\partial R}{\partial X_2} \delta X_2 \right)^2 + \dots \dots \dots \left( \frac{\partial R}{\partial X_n} \delta X_n \right)^2 \right]^{1/2} \quad (23)$$

In Equation (23), the partial derivative of R with respect to its X is the sensitivity coefficient for the result R with respect to its measurement X.

The zeroth order uncertainty is used for planning the experiment by suggesting the selection of the instrumentation to be used. The first order uncertainty is helpful during the debugging phase of the experiment. The Nth order uncertainty interval estimates the overall uncertainty in the result, including the effect of all the fixed and the variable errors. It should, however, not be used to assess the scatter on repeated trials with the same instruments, since it includes the fixed errors that cannot contribute to the scatter on the repeated trials.

Moffat (1988), explains the multiple sample uncertainty analysis in reference to ASME PTC 19.1 – 1985. Chapter 2, introduction to uncertainty analysis explains in detail about the multiple sample uncertainty analysis referred from ASME PTC 19.1 – 2005. The multiple sample uncertainty consists of two errors systematic/bias error which is given by the instrumentation, and precision/random error obtained from the standard deviation. These two errors give the systematic and random uncertainty using RSS. And finally these two uncertainties are combined using RSS to get the total uncertainty.

Uncertainty calculated by using both single and multiple samples provides results with negligible difference. Hence the choice of utilizing single or multiple sample uncertainty depends on the objective and therefore each has its own different structure.

In regards to heat transfer and turbomachinery, Lavagnoli, Maesschalck and Paniagua (2015), provided a detailed analysis of the measurement uncertainties associated with the relevant parameters that drive the convective thermal process in transient turbine experiments. Their research quantifies the error in the measured or calculated local gas temperature and convective heat transfer coefficient.

The work of Yao, Chen, Luo, Tooren and Guo (2011), their work is about using uncertainty analysis for multidisciplinary optimization methods for aerospace vehicles. Figure 3-2 show the flow process developed for uncertainty based multidisciplinary optimization.



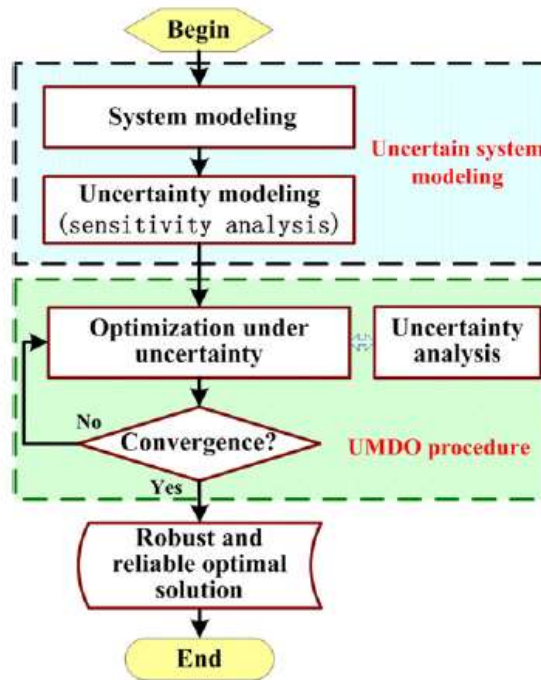


**Figure 3-2: Uncertainty-Based Multidisciplinary Design Optimization (UMDO) (Yao et al., 2011)**

From Figure3-2, the uncertainty system modelling consists of system modelling and uncertainty modeling. The system modelling includes the mathematical model for the optimization problems such as design variables, optimization objectives, constraints, design space, etc. The uncertainty modeling is the quantification and classification of uncertainty involved in the system design. There are a vast number of uncertainties in the aerospace vehicle design which will lead to unacceptable calculation burden. Hence a sensitivity analysis is done to separate out the factors which have no significance influence in the system design.

Optimization with uncertainty analysis is done to save time and resources, thus increasing the reliability and robustness of the design.

Tai and Mines (2016), demonstrate a process for quantifying the uncertainty related to meeting performance early in the conceptual design of an aircraft engine to avoid

cancellation in the preliminary design phase. Figure 3-3 gives about the approach for Uncertainty Quantification and Management (UQ&M) process.

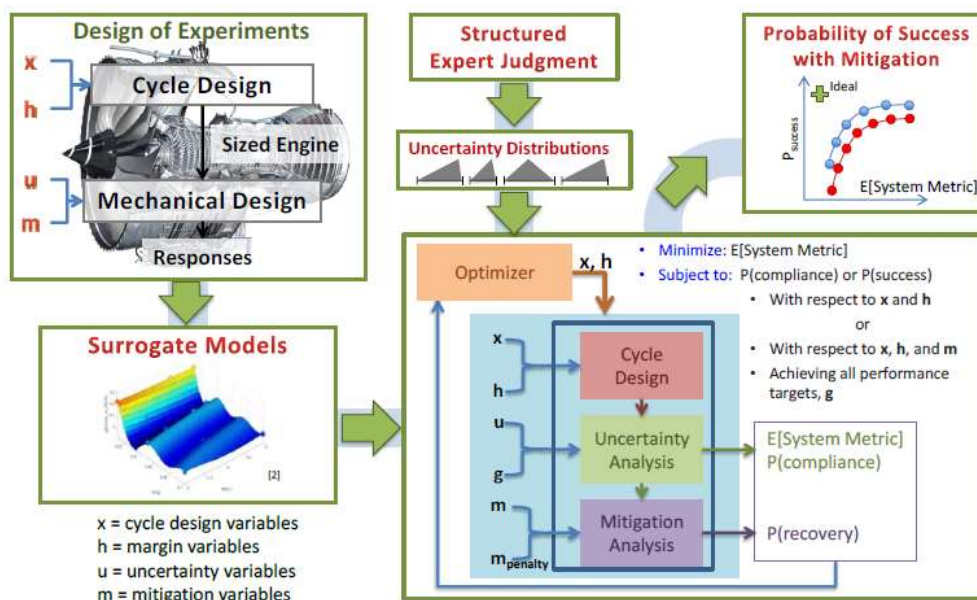


**Figure 3-3: Technical Approach (Tai and Mines, 2016)**

The variables are grouped into four categories. Design variables ( $x$ ) are the deterministic sizing parameters under the control of the designer, common examples include pressure ratio, temperature limits, flow rate, etc. Margin variables ( $h$ ) are adders or multipliers on system, such as the temperature margins of the material. Mitigation variables ( $m$ ) are used to correct the missed lower level target or constraint, they may overlap with design variables, generally represent variables that can be changed during operation or can be changed late in the design. Random variables ( $u$ ) are the uncertainty parameters which are outside the designer's control and will affect the performance of the system. Using surrogate models, the reliability analysis is performed for the fixed parameters with respect to its uncertainty variable to calculate the probability of meeting the system level performance targets. If the target is not achieved the mitigation variables are applied to recover the design this is called as the mitigation analysis.

The importance of uncertainty is depicted by different literature reviews. Robert J. Moffat (1988) said it is no longer acceptable, in most circles, to present experimental results without describing the uncertainties involved. Uncertainty analysis provides the experimenter a rational way of evaluating the significance of the results, which can be a powerful tool to locate the source of error in an experiment.

### 3.2 Optimized Ribs

For rib turbulated channel cooling, the ribs were optimized using Optimate + in STAR CCM + and were studied numerically using CFD by the IGNITE research team Ranade, Gutierrez, Guillen, Mehta & Ricklick (2016) in Embry Riddle Aeronautical University. Various rib designs were studied in which three were published in accordance to best performance in Nu, pressure drop and thermal efficiency. Figures 3-4, 3-5 and 3-6 describe the turbulated flow feature by the rib in a rectangular channel.

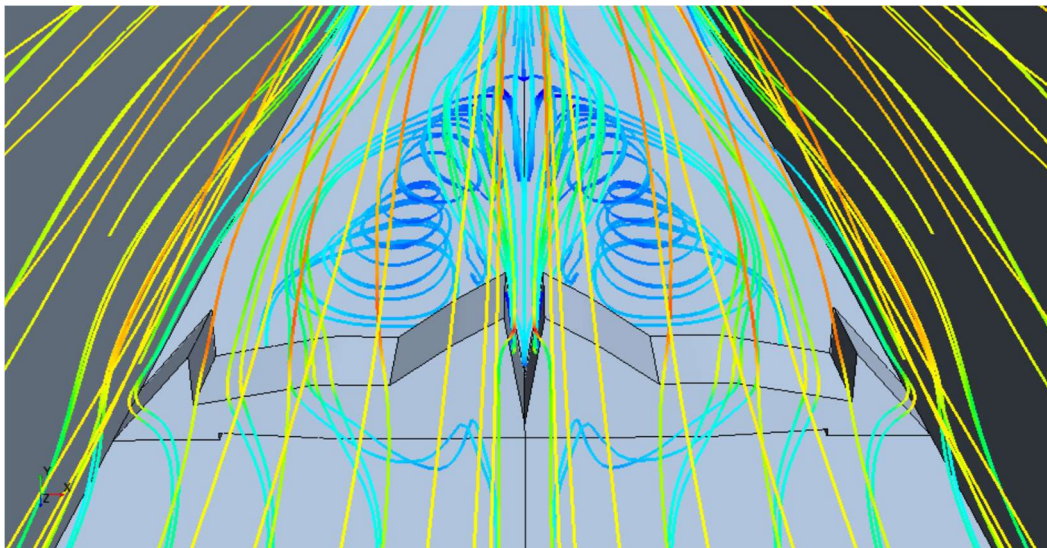


**Figure 3-4: Flow feature of rib 1 (Ranade et al., 2016)**

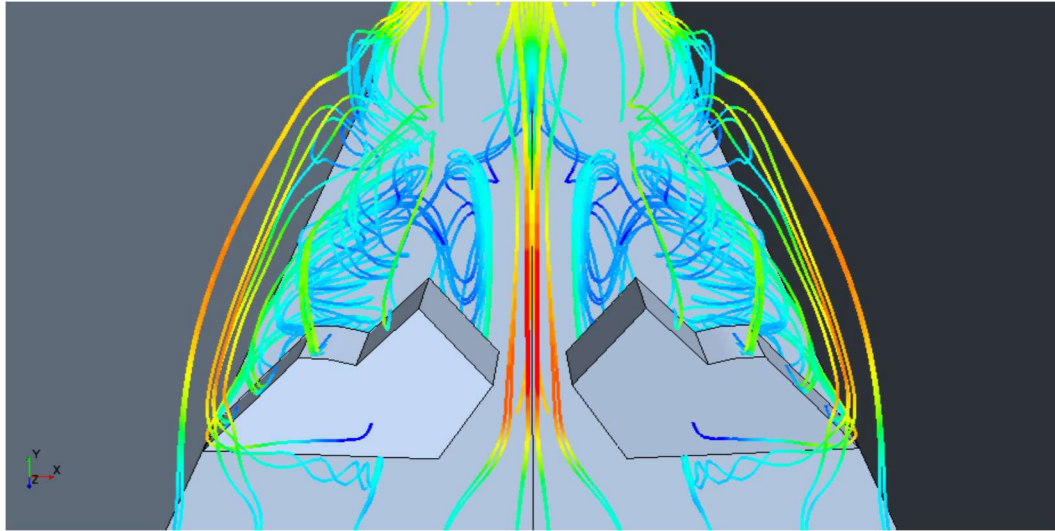


**Figure 3-5: Flow feature of rib 2 (Ranade et al., 2016)**

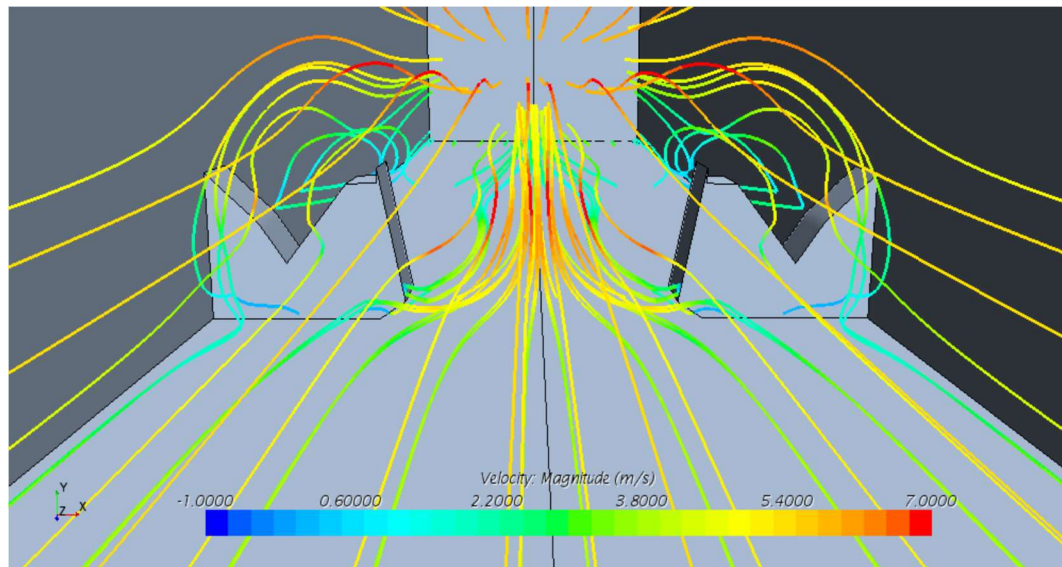


**Figure 3-6: Flow feature of rib 3 (Ranade et al., 2016)**

Rib 1 was found to be performing better overall and the uncertainty analysis for the rib channel was conducted using a 3D printed rib 1. All three ribs are analyzed experimentally and compared with the numerical results.

#### 4. Problem Statement and Objective

The literature does not explain the sample size required to perform an uncertainty analysis in a heat transfer experiment. The hypothesis of this research is that using a smaller number of samples will not result in a statistically different uncertainty in comparison to the uncertainty based on larger number of samples.

The primary objective of this research is to reduce the uncertainty in a propulsion heat transfer experiment at Embry Riddle Aeronautical University. In relation to the primary objective, three studies are done. Under first study as described in Figure 4-1 the first step is to determine the major contributing factor to the uncertainty using a developed tool. Then determine the best method to reduce the uncertainty for that major contributing factor.

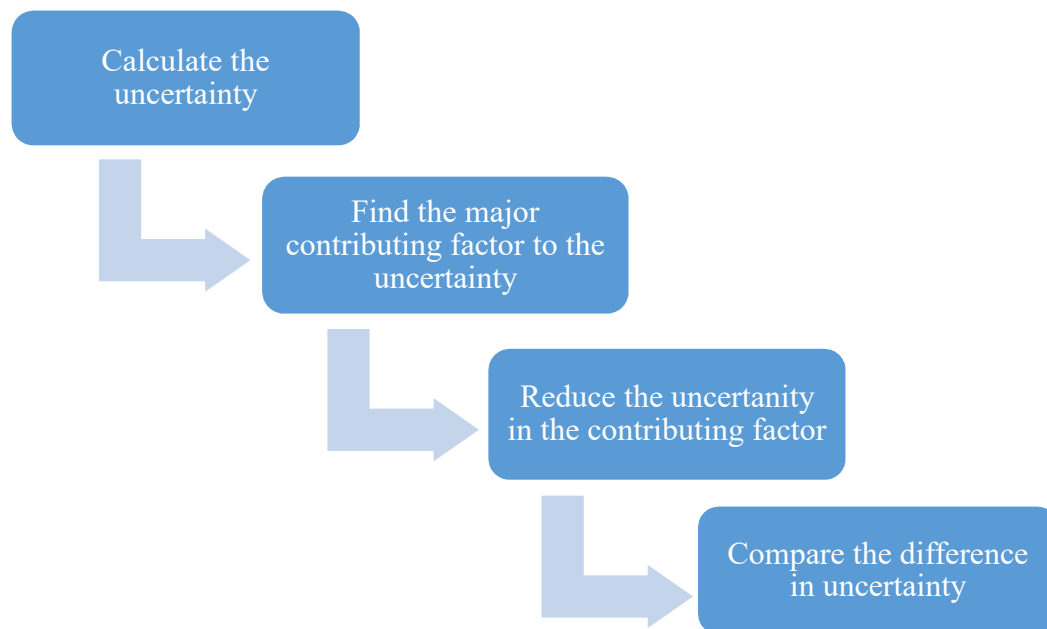


**Figure 4-1: First study of primary objective**

Second, study the effect of temperature difference between surface and bulk temperature( $\Delta T$ ) in contribution to the final uncertainty. And third confirm the uncertainty

using student's t distribution with a fewer number of samples is a viable option to neglect using a normal distribution (larger number of samples). This will reduce the times that the experiment needs to be repeated and improves the cost effectiveness of the testing method.

The secondary objective is to experimentally analyze the three optimized ribs and compare them with respect to average Nu and pressure drop for different Re. Find out the better performing rib and compare it to the result of numerical analysis from the literature.

## 5. Data Reduction

### 5.1 Introduction to Heat Transfer

#### 5.1.1 Conduction Heat Transfer

When there is a temperature gradient in a body, there is an energy transfer from the high-temperature region to the low-temperature region. Therefore, by this statement energy is transferred through conduction and the heat transfer rate per unit area is proportional to the normal temperature gradient given by the Fourier's conduction law,

$$\frac{q_x}{A} = -k \frac{\partial T}{\partial x} \quad (24)$$

Where  $k$  is the thermal conductivity of the material. The negative sign indicates the direction of energy flux.

#### 5.1.2 Convection Heat Transfer

It is well known that a hot plate of metal will cool faster in the presence of air flow than in still air. The heat is convected away, and this process is called as convection heat transfer. There are two types forced convection and natural convection, in our case we use forced convection. To express the overall effect of convection, Newton's law of cooling is used, which is given by the relation,

$$q = hA(T_w - T_\infty) \quad (25)$$

Where  $h$  is the heat transfer coefficient, sometimes called film conductance. Figure 5-1 explains about the schematics of convection which is the base for the experiment conducted.



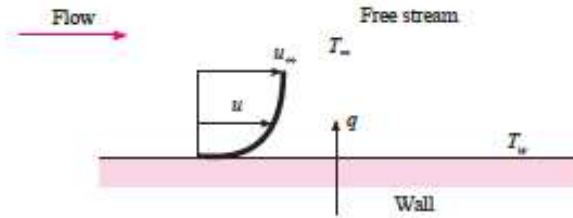


**Figure 5-1: Convection heat transfer from a plate (J.P. Holman)**

The Flow is characterized by Reynolds number (Re), which is given by the relation,

$$Re = \frac{\rho v L^*}{\mu} \tag{26}$$

Where  $L^*$  is the characteristic length of the region in use and varies in accordance to open and closed channel.

To non-dimensionalize the level of convective heat transfer, Nusselt number (Nu) is utilized. It is given by the relation,

$$Nu = \frac{h L^*}{k} \tag{27}$$

Here  $k$  is the thermal conductivity of air and  $L^*$  is the characteristic length of the region in use. The data reduction steps taken to calculate Nu is given by the Figure 5-2.

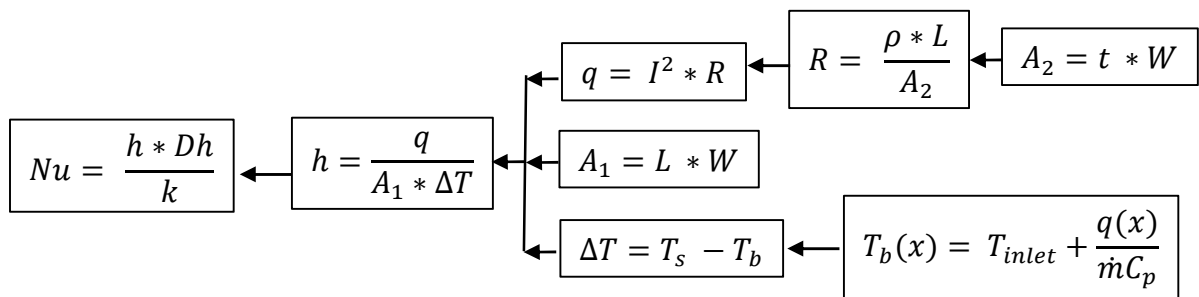


**Figure 5-2: Variable Cascade for Nusselt Number**

The final uncertainty in Nu is calculated through the propagation of error from each term that is required to calculate Nu. Using Figure 5-2, the error propagates from the right through each term and finally ends at Nu at the left.



## 5.2 Uncertainty Data Reduction

Multiple sample uncertainty method is used in this analysis as it best suits the objective. For this research in calculating the uncertainty, the length, width, height and resistance are kept constant and these will not contribute to the uncertainty.

Current is measured using the ammeter in the VARIAC. Since mean value of the measurements is used in calculating the uncertainty, the bulk temperature ( $T_b$ ) will be the average of inlet and outlet temperature. These temperatures are measured using the type T thermocouple with a digital thermometer. The surface temperature ( $T_s$ ) is taken to be the mean surface temperature from post processing using a code in MATLAB.

As discussed in the section 2.4.2 RSS method is used in calculating the uncertainty.

Hence the uncertainty of Nu is calculated by,

$$b_{Nu} = \sqrt{\left(\frac{\partial Nu}{\partial h} * b_h\right)^2 + \left(\frac{\partial Nu}{\partial k} * b_k\right)^2} \quad (28)$$

$$S_{Nu} = \sqrt{\left(\frac{\partial Nu}{\partial h} * S_h\right)^2 + \left(\frac{\partial Nu}{\partial k} * S_k\right)^2} \quad (29)$$

$$u_{Nu} = \sqrt{b_{Nu}^2 + S_{Nu}^2} \quad (30)$$

$$U_{Nu} = t_{95} * u_{Nu} \quad (31)$$

The error in Nu is dependent on the errors of h and k, affected by their sensitivity coefficient. The variables h and k will have their own systematic and random uncertainties, and the same RSS method is used to calculate them.

The thermal conductivity (k) is calculated from the correlation based on Sutherland's equation (McQuillan, Culham and Yovanovich, 1984). The equation for k is given as,

$$k = \frac{2.3340 * 10^{-3} * T^{1.5}}{164.54 + T} \quad (32)$$

In this equation the Temperature (T) is taken as the bulk temperature of the air in kelvin. Therefore, the systematic and random uncertainty are given as,

$$b_k = \sqrt{\left(\frac{\partial k}{\partial T_b} * b_{T_b}\right)^2} \quad (33)$$

$$S_k = \sqrt{\left(\frac{\partial k}{\partial T_b} * S_{T_b}\right)^2} \quad (34)$$

Furthermore, the error in variable h is dependent on the errors of heat transfer rate (q) (q depends on current (I)), and  $\Delta T$  (difference between surface to bulk temperature), neglecting the errors in surface area and resistance (R) since they are kept constant. With each variable has its own systematic and random uncertainty, given in APPENDIX A.

### 5.2.1 Heat Leakage

In ideal case all the heat applied by the strips will be convected by the air flow, but acrylic is not a perfect insulator, hence the heat will leak through the acrylic into the surrounding, which should be accounted for in calculating the effective heat supplied.

$$q = (I^2 * R) - (m * (T_s - T_{inlet}) * A_1) \quad (35)$$

Where m is the slope calculated from the heat leakage test described in section 6.4.1. Then the systematic and random uncertainty will be calculated as

$$b_q = \sqrt{\left(\frac{\partial q}{\partial I} * b_I\right)^2 + \left(\frac{\partial q}{\partial T_s} * b_{T_s}\right)^2 + \left(\frac{\partial q}{\partial T_{inlet}} * b_{T_{inlet}}\right)^2} \quad (36)$$

$$S_q = \sqrt{\left(\frac{\partial q}{\partial I} * S_I\right)^2 + \left(\frac{\partial q}{\partial T_s} * S_{T_s}\right)^2 + \left(\frac{\partial q}{\partial T_{inlet}} * S_{T_{inlet}}\right)^2} \quad (37)$$

### 5.2.2 Reynolds Number

Re is calculated using mass flow rate, hydraulic diameter, cross-sectional area of the channel and dynamic viscosity, in which the values of hydraulic diameter and cross sectional area is kept constant. The formula is given by

$$Re = \frac{\dot{m}D_h}{A_c\mu} \quad (38)$$

The mass flow rate is calculated using measurements obtained from the venturi-meter and the dynamic viscosity is calculated by

$$\mu = \nu\rho \quad (39)$$

The variable  $\nu$  is the kinematic viscosity. The density is calculated from the ideal gas law, and the pressure used in the ideal gas is the atmospheric pressure of air.

$$\rho = \frac{P}{RT} \quad (40)$$

Where R is the gas constant. The systematic and random uncertainty for Re are calculated by the propagation of error from each calculated measurement using RSS, given in APPENDIX A.

### 5.2.3 Pressure Drop ( $\Delta P$ )

Pressure drop across the channel is measured from a manometer with a resolution of 0.02 inch of water. Since it is a single measurement, RSS for a single measurement uncertainty, as mentioned in section 2.4.1, is used to calculate the systematic and random uncertainties, given in APPENDIX A.

## 6. Experimental Model

### 6.1 Experimental Setup

The end wall of the acrylic is painted with a uniform coat of TSP, above which the strips are placed using a double sided thermal conducting tape. The strips are connected in series using copper bus bars. These are then connected to a VARIAC to form a series circuit. The rib in case of rib channel, or pin fins in case of pin fin channel is placed on the inconel heater strips using the double sided tape, see Figure 6-1.

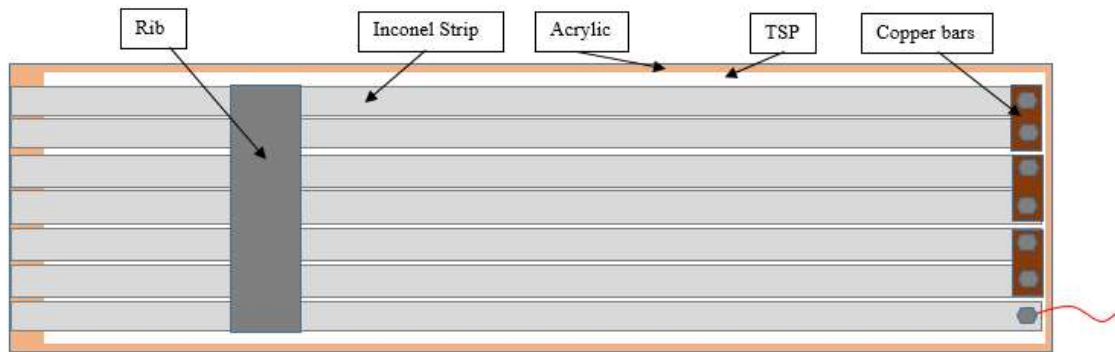


**Figure 6-1: Schematic of wall setup**

Figure 6-2 shows the experimental setup of the pin fin channel, which is similar to the rib channel with just the replacement of rib with the pin fins. A scientific grade CMOS camera is used to capture the TSP, which is excited by ultra violet light.

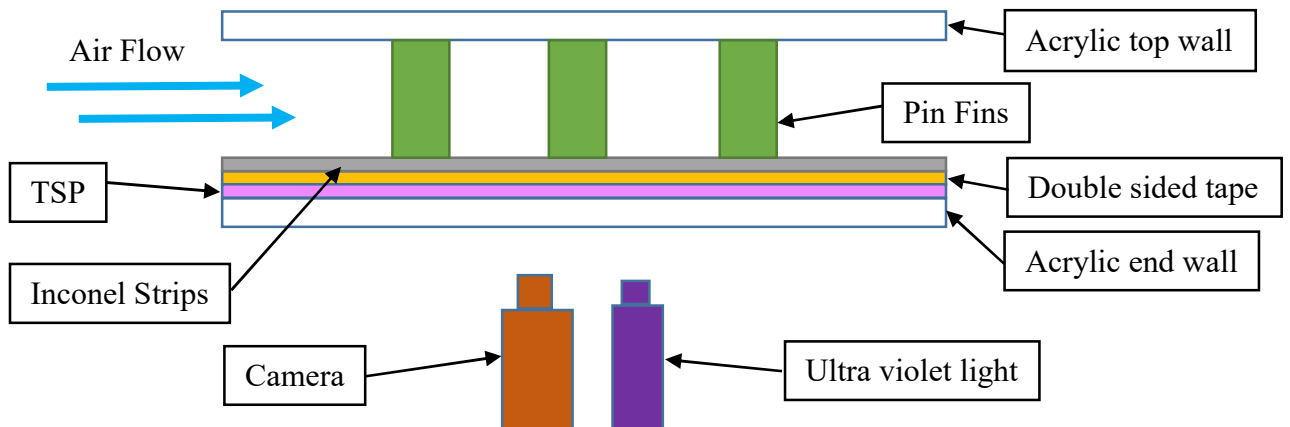


**Figure 6-2: Schematic of experimental setup**

## 6.2 TSP Setup

The TSP paint is applied in layers to form a thin or thick coat, depending upon requirement. Sufficient time is given to dry before applying each layer. After applying the TSP on the test piece, it is then placed in a dark room to prevent degradation, as the quality of the paint slowly degrades when exposed to light. It is left for a full day to completely dry, then the paint is heat treated for activation. Figure 6-3 shows a test piece with its surface coated with TSP.



**Figure 6-3: TSP on a test piece**

## 6.3 Intensity Validation

The intensity of the ultra violet used to excite the TSP molecules varies with time. The intensity will be high when the light source is switched on, and decreases gradually to become eventually constant. An intensity validation test was conducted to determine the proper time interval to keep the light on before taking readings. The intensity values are obtained from the image taken of the TSP using a scientific grade camera for 1ms exposure time.

From Figure 6-4 it is observed that the intensity of the light steadies after 15 minutes. Therefore, initial reading should be taken after 15 minutes. If this is neglected the intensity recorded will be higher than the correct value. This will affect the post processed value of surface temperature from the calibration curve of TSP, and increase the error of TSP.

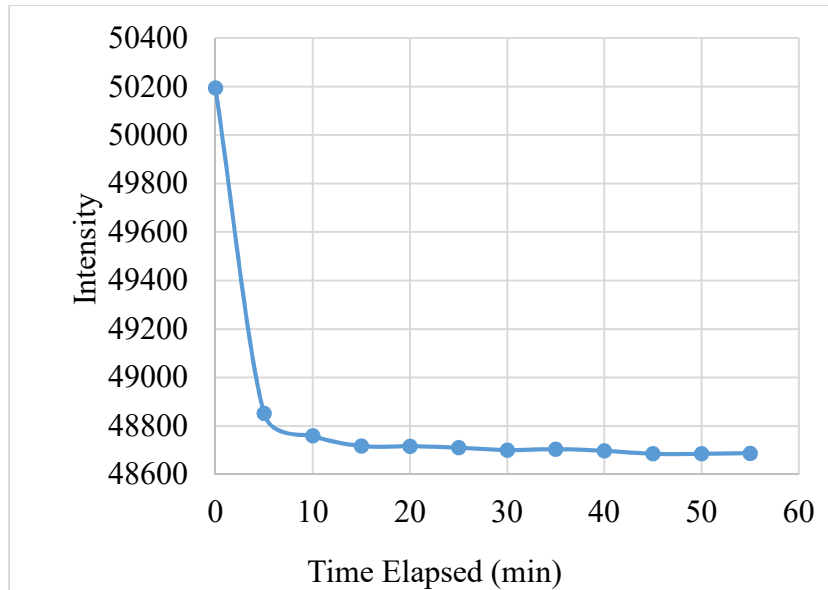


**Figure 6-4: Intensity validation (Pai, 2016)**

#### **6.4 Rib Channel**

The experimental apparatus is setup in a way that the back side of the acrylic plate which is transparent to the TSP is kept facing the ultraviolet light and the camera as shown in Figure 6-5. The camera and the ultraviolet light are mounted on the traverse for flexibility. The whole setup is kept inside a dark room.

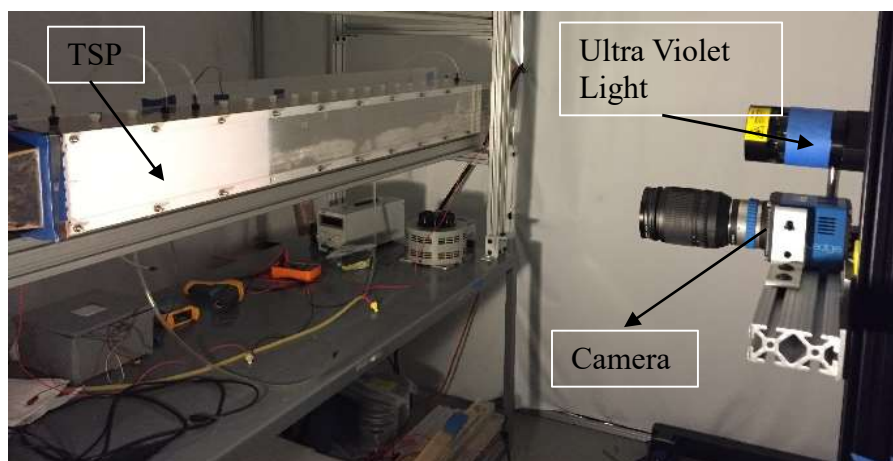


**Figure 6-5: Rib channel**

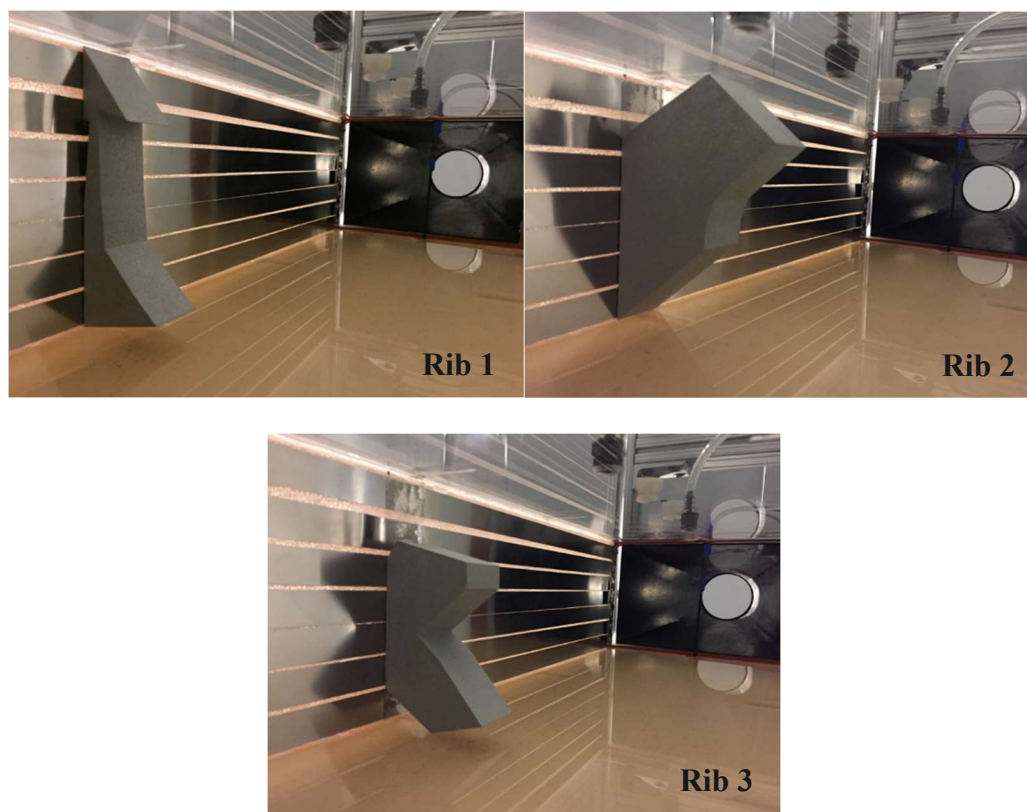


**Figure 6-6: Optimized ribs**

Figure 6-6 shows the optimized ribs which are used for experimental analysis. Among the three ribs, rib 1 is used for the uncertainty analysis.

### 6.4.1 Heat Leakage Test – Rib Channel

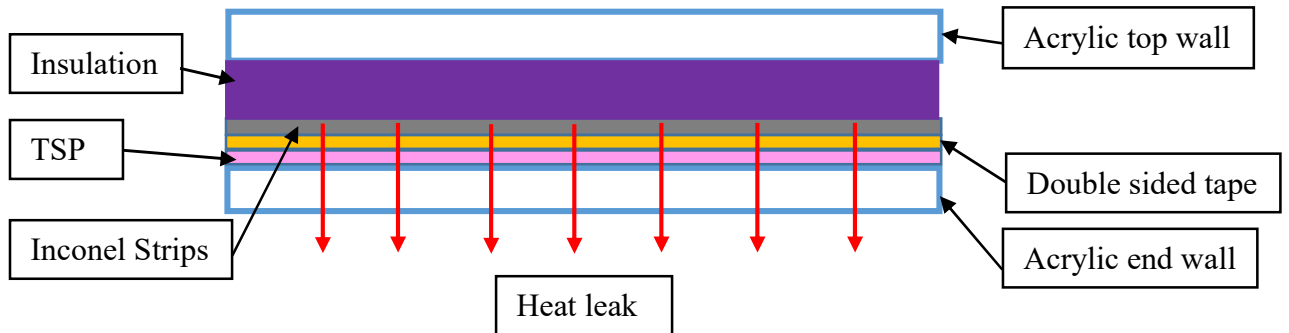


**Figure 6-7: Schematic of heat leak test**

Figure 6-7 shows a schematic of heat leakage test. The acrylic end wall used is not a perfect insulator, therefore when the end wall is heated by the heater strips some percentage of heat leakage is expected through the end wall into the surroundings. A heat leak test is conducted by covering the top surface with insulation to make sure the leakage occurs only through the end wall. A plot between heat flux supplied and the temperature difference (from a thermocouple placed on the heater strips and on the other side of the end wall) is made, see Figure 6.8.

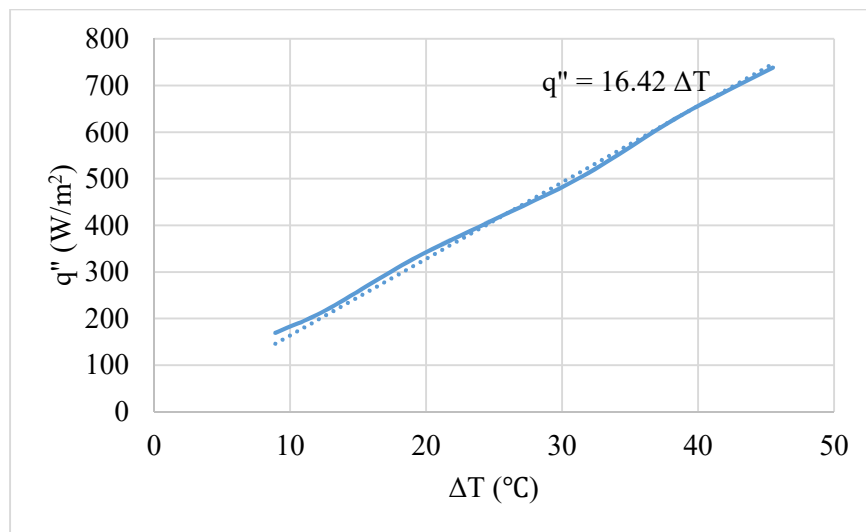


**Figure 6-8: Heat leakage test - rib channel**



From Figure 6-8 the heat leakage slope is obtained and the effective heat flux is calculated by,

$$q''_{effective} = q''_{supplied} - q''_{leaked} \quad (41)$$

$$q''_{effective} = \frac{I^2 R}{A_1} - (16.42 * \Delta T) \quad (42)$$

#### 6.4.2 Smooth Channel Test – Rib Channel

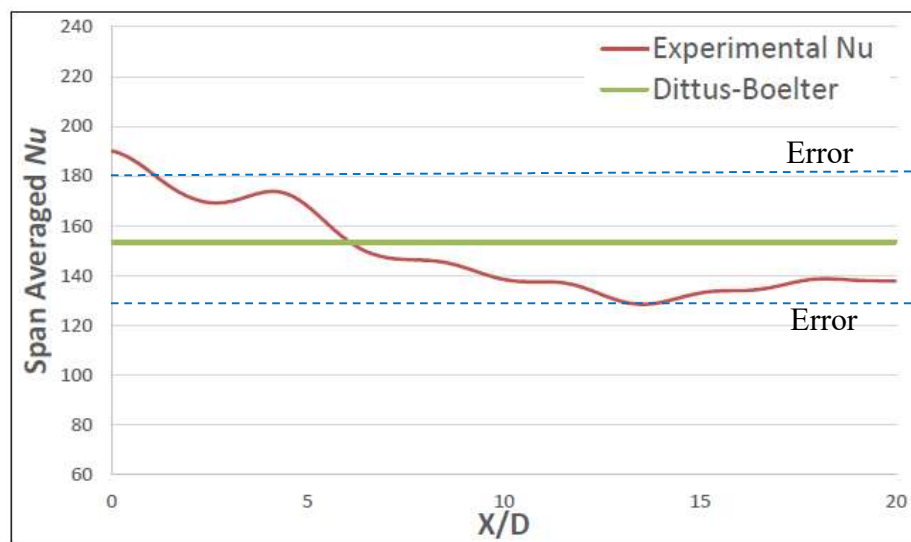


**Figure 6-9: Smooth channel test – rib (Upalkar, 2015)**

From Figure 6-9, on comparing the smooth channel test done by Upalkar on the same rig utilized in these experiments, with that of Dittus-Boelter, the profile matches within 12% error in the fully developed region, which establishes the experimental setup to be valid.

## 6.5 Pin Fin Channel

Similar to the rib channel setup the back side is kept facing the camera and the ultraviolet light as shown in Figure 6-10. Figure 6-10 also shows the front section of the channel with a bank of pin fins rested on top of Inconel strips placed carefully much closer to each other, to get a better temperature and Nu contour in post processing.

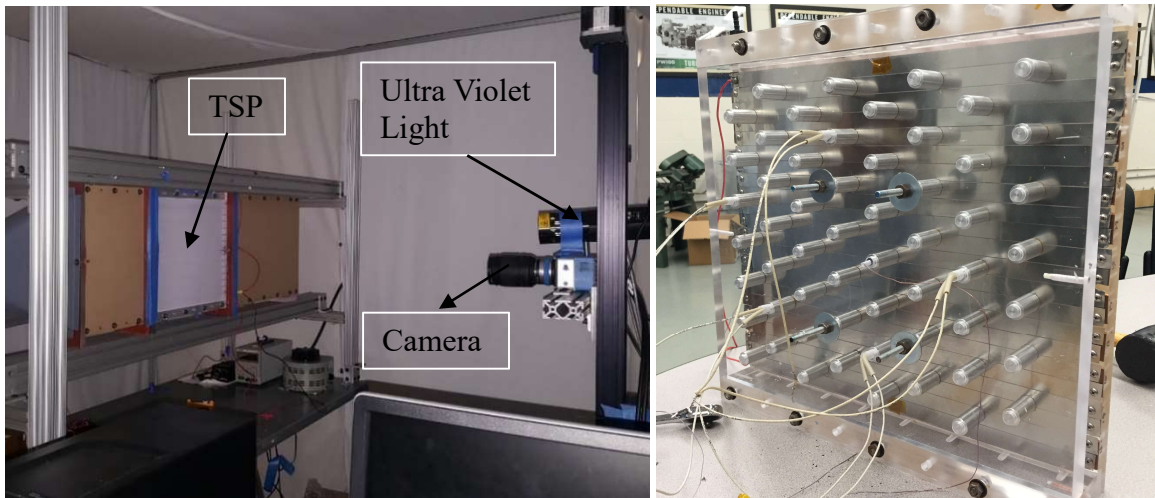


**Figure 6-10: Pin fin channel**

### 6.5.1 Heat Leakage Test – Pin Fin Channel

As explained in section 6-4.1 a heat leak test was also conducted to the pin fin channel to determine the amount of heat leaked to the surrounding through the acrylic plate, as shown in Figure 6-11.

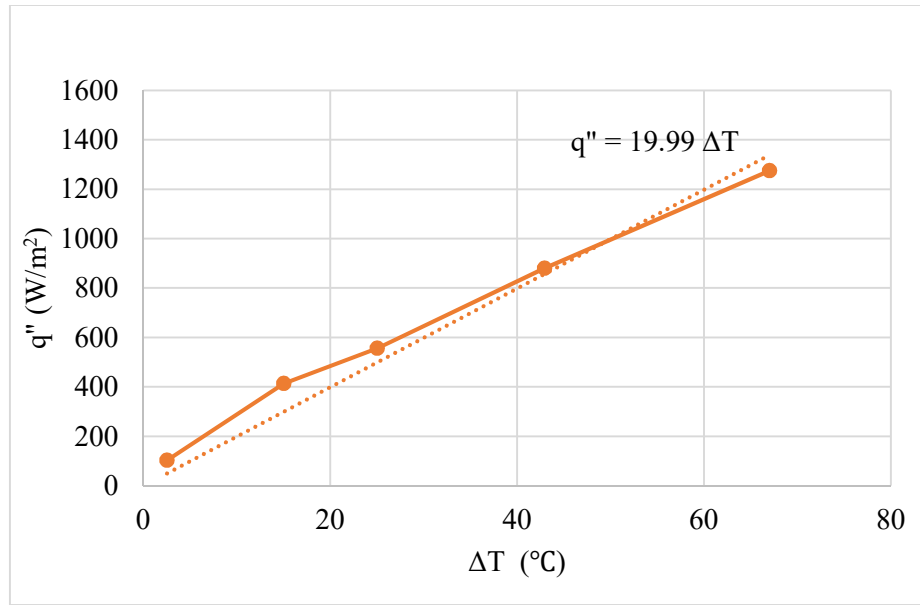


**Figure 6-11: Heat leak test – pin fin channel**

### 6.5.2 Smooth Channel Test – Pin Fin Channel

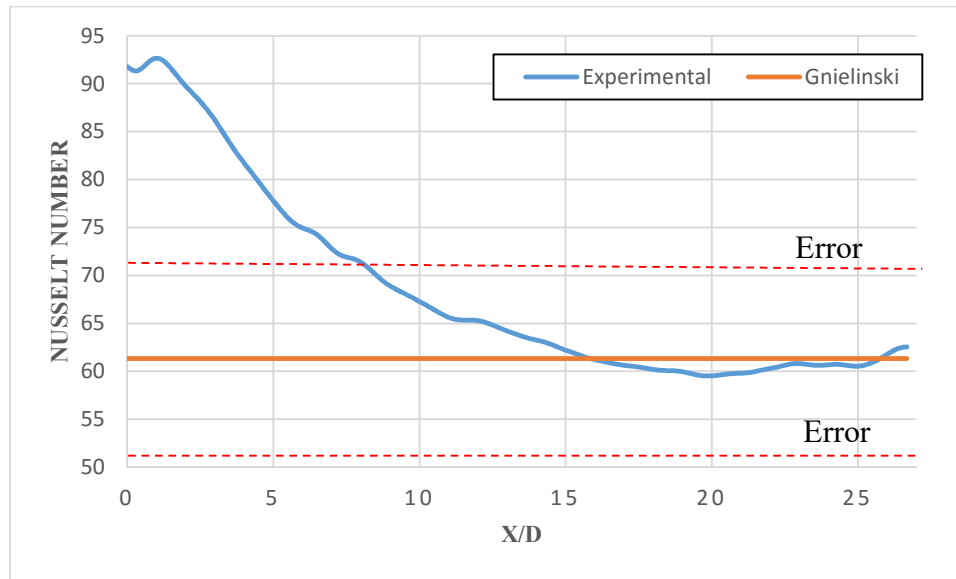


**Figure 6-12: Smooth channel test – pin fin (Fernandes, 2016)**

From figure 6-12 on comparing the smooth channel test done on the pin fin channel with respect to Gnielinski, the span wise average Nusselt number profile matches within the 20% error range of Gnielinski in the fully developed region.

## 7. Uncertainty Analysis

### 7.1 Rib Channel

Rib 1 as shown in section 6.4 was used in the uncertainty analysis. Figure 7-1, 7-2, 7-3 shows the temperature contour, Nu contour, and the span-wise Nu of Rib 1 for Re of 70000 and heat flux of 1300 W/m<sup>2</sup>.

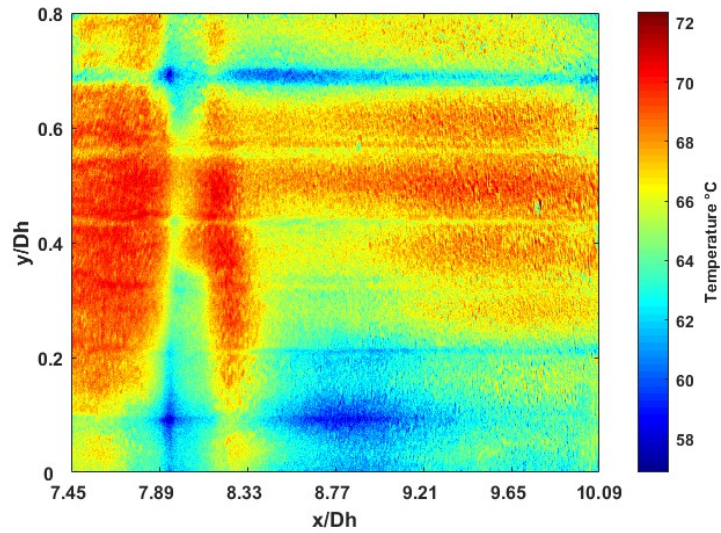


Figure 7-1: Temperature contour

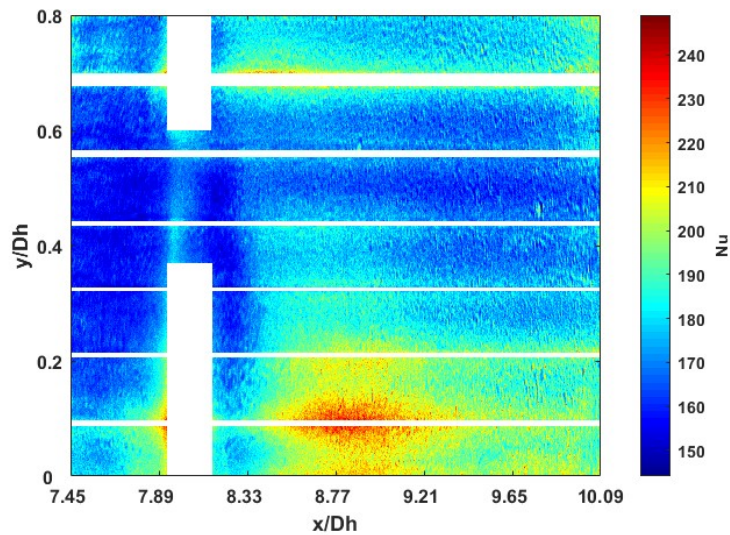
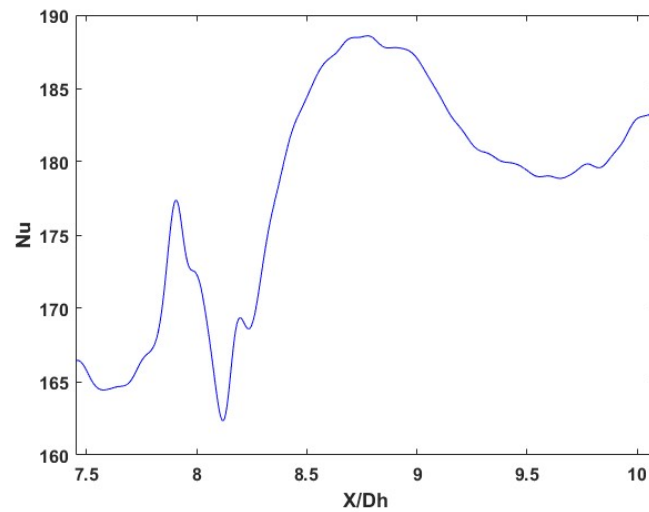


Figure 7-2: Nu contour



**Figure 7-3: Span-wise average Nu**

The characteristic length is taken as the channel hydraulic diameter which is 0.15m and the pressure drop was measured to be 5.729 Pa. It is seen from Figure 7-2 that the Nu is higher in the region of the vortex created by the rib, since it involves more heat transfer. The area between the strips and under the rib are neglected as can be seen in Figure 7-2, for a proper calculation in span wise average Nu.

### 7.1.1 Student's t Distribution (N=5) – Rib Channel

The experiment was repeated 5 times. Between each repetition the experiment was switched off and started from the beginning to check for repeatability. The bias error from each measuring device is taken from the manufacturer of the recording devices used. The error for the TSP measurement is assumed to be 2 ° C, since the calibration uncertainty of TSP was found to be  $\pm 0.93$  ° C (Liu, 2006). The bias errors for the various devices are given below:

- VARIAC (for current measurement)
  - Resolution = 0.01

- Error in current measurement = 1% of reading
- Least Significant Digit (LSD) = 0.02
- Accuracy = 1% of reading  $\pm$  LSD
- Thermocouple
  - Error =  $\pm$  1 °C
- Digital Thermometer
  - Resolution = 0.1
  - Error =  $\pm$  0.05% of reading
- Surface Temperature (TSP – Assumed)
  - Error =  $\pm$  2 °C

Table 7-1 gives the measurement taken 5 times with mean and standard deviation for the calculation of Nu.

**Table 7-1: Measurements for Nu calculation**

Data	I (A)	T <sub>s</sub> (°C)	T-inlet (°C)	T-outlet (°C)
1	5.95	66.233	22.7	22.9
2	6.08	68.007	22.7	22.9
3	6.09	68.048	22.5	22.7
4	6.12	68.539	22.5	22.7
5	6.13	68.733	22.3	22.5
Mean	6.074	67.912	22.54	22.74
Std-Dev	0.072319	0.989133	0.167332	0.167332

Using the mathematical model, the mean Nu was calculated with its uncertainty.

- Nu = 176.09
  - Error =  $\pm$  15.42,  $\pm$  14.09
  - Error percentage = 8.75 %, 8.01 %

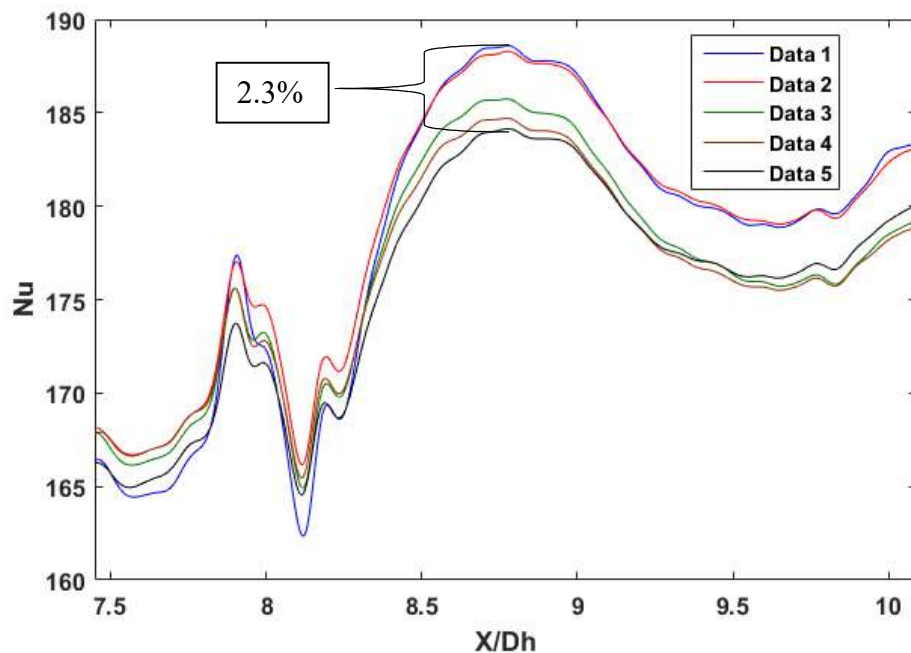


**Figure 7-4: Span-wise average Nu comparison**

From Figure 7-4 the span-wise average Nu lines ideally should lie on top of each other, but due to error in measurements there is a deviation from one to other with a maximum difference of 2.3%. Using the explanation given in section 2.6 the contributing factor to the uncertainties are calculated and presented in Figure 7-5, 7-6, 7-7, 7-8.

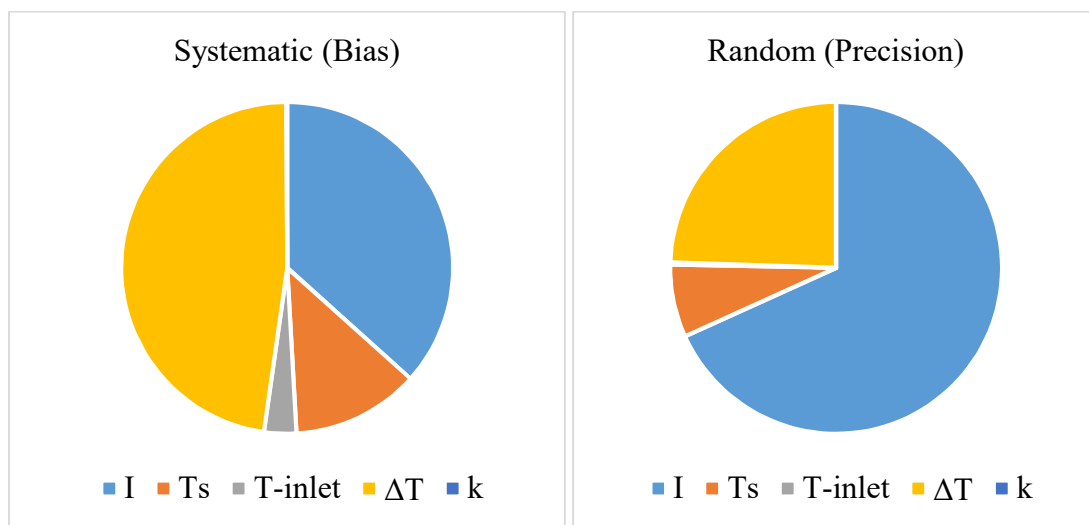


**Figure 7-5 Uncertainty contribution in Nu**

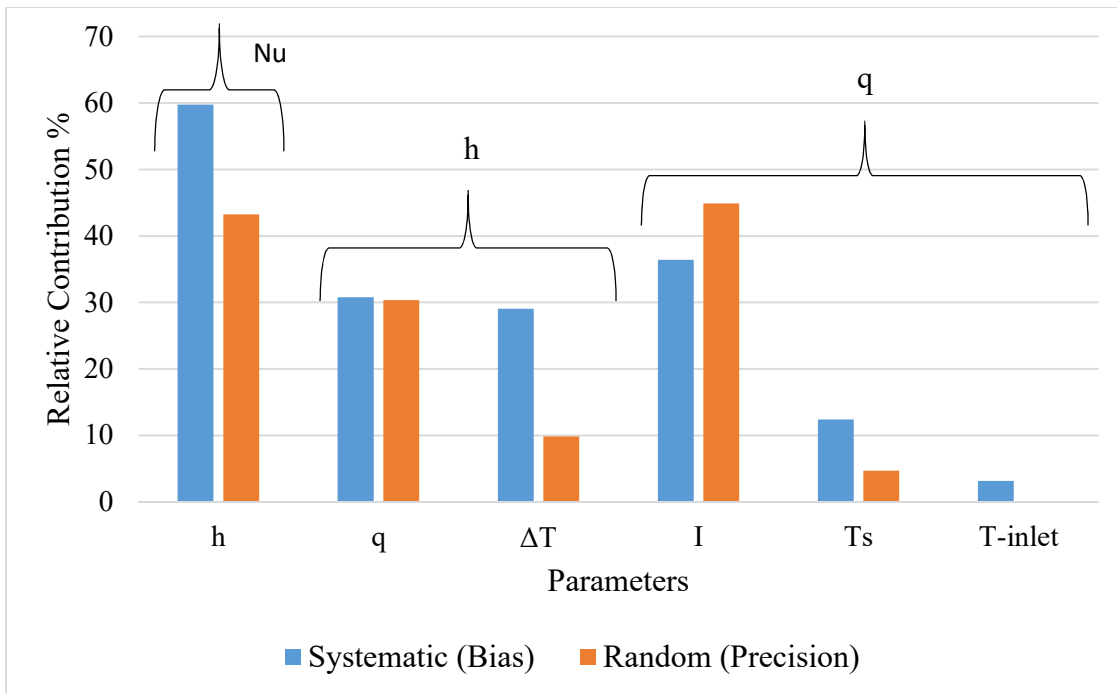


Figure 7-6: Uncertainty contribution in Nu, h, q

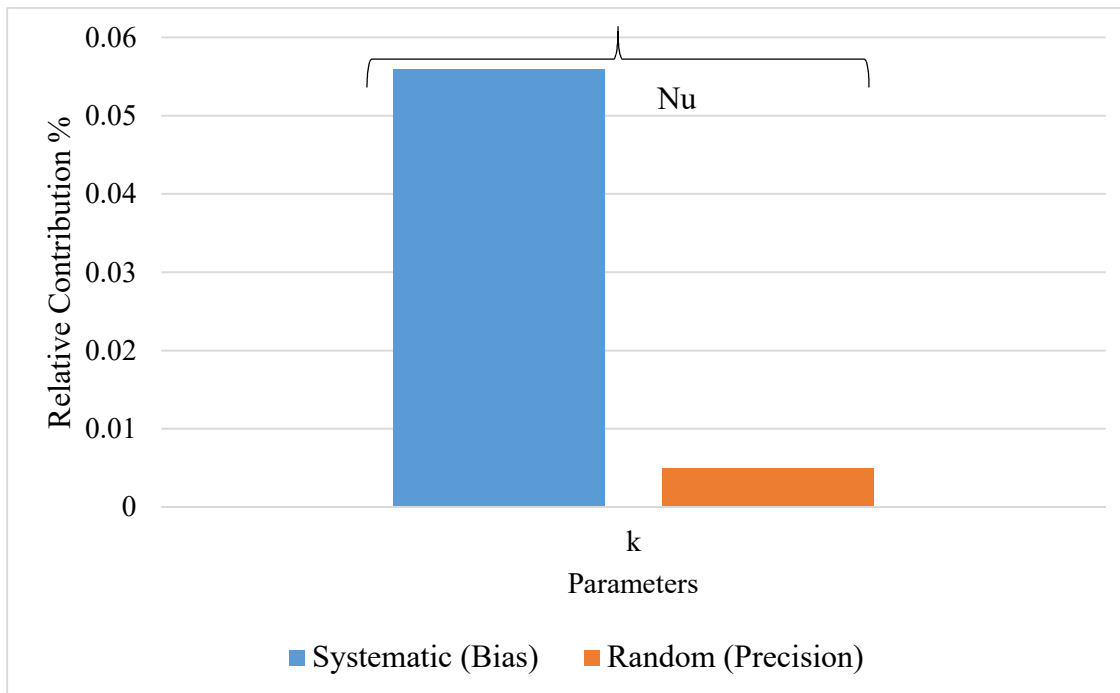
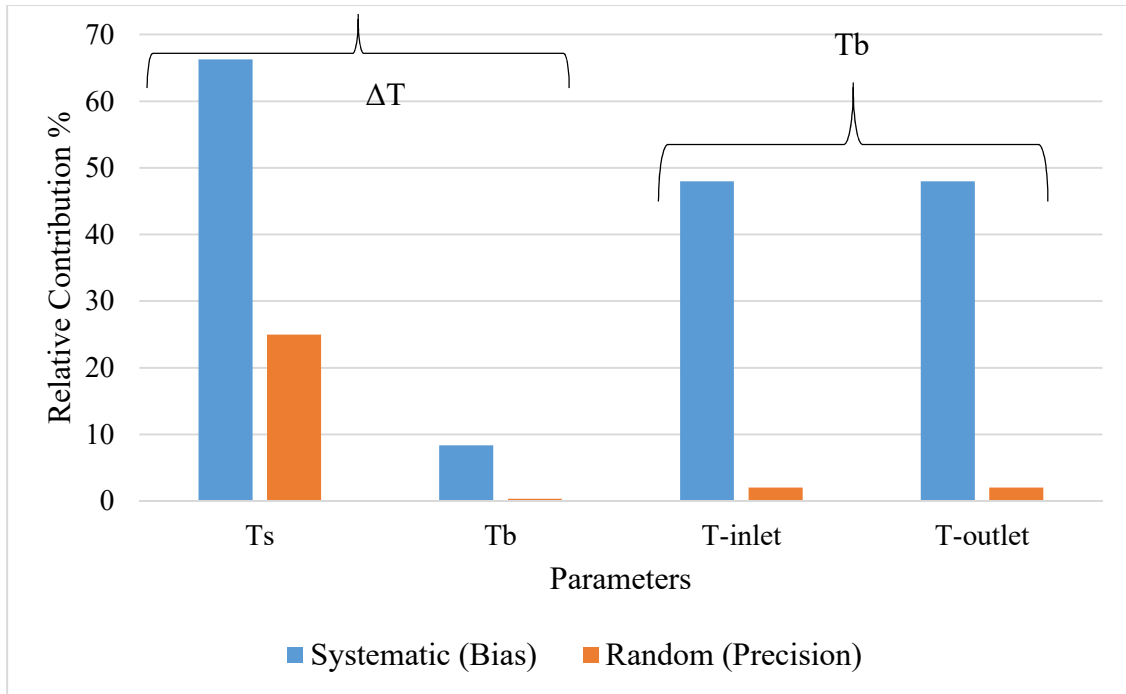


Figure 7-7: Uncertainty contribution in thermal conductivity





**Figure 7-8: Temperature contribution to uncertainty.**

Figure 7-5 shows the relative contribution of uncertainties in Nu, which is given by the relation,

$$Nu = \frac{\left(\frac{I^2 R}{A_1} - (16.42 * (T_S - T_{inlet}))\right) * D_h}{\Delta T * k} \quad (43)$$

From Figure 7-5, the current (I) has a high systematic and random uncertainty contribution. The  $\Delta T$  has a high systematic uncertainty contribution, higher than the current. Its contribution is explained in detail in section 7.3.2. Thermal conductivity (k) has negligible contribution.

Figure 7-6, 7-7, 7-8 show the relative contribution of uncertainties to its respective parameter used in calculating the Nu. For example, h and k will together have an 100% relative contribution to the uncertainty in Nu, given by the relation,

$$1 = \frac{\left(\frac{\partial Nu}{\partial h} * B_h\right)^2 + \left(\frac{\partial Nu}{\partial k} * B_k\right)^2 + \left(\frac{\partial Nu}{\partial h} * \bar{S}_h\right)^2 + \left(\frac{\partial Nu}{\partial k} * \bar{S}_k\right)^2}{u_{Nu}^2} \quad (44)$$

The relative contribution of h to the systematic uncertainty of Nu is calculated by dividing  $\left(\frac{\partial Nu}{\partial h} * B_h\right)^2$  by  $u_{Nu}^2$  and multiplying by 100. Similar approach is followed for the remaining variables.

From Figure 7.7 it is seen that contribution of k is negligible. From Figure 7-6 the heat transfer coefficient (h) contributes high in terms of both systematic and random uncertainty in the calculation of Nu parameter. With respect to h, the heat transfer rate (q) with heat leakage is the highest uncertainty contributor and among (q) the current (I) is the highest uncertainty contributor. From Figure 7-8 the systematic uncertainty of surface temperature (Ts) is high due to high assumed error for TSP. Therefore, it is found that current measured from the VARIAC is the main contributor to the uncertainty.

Uncertainty in Re and pressure drop were also calculated. Table 7-2 gives out the measurements used to calculate the uncertainties.

**Table 7-2: Measurements for Re calculation and pressure drop ( $\Delta P$ )**

Data	Atm-P (Pa)	$\dot{m}$ (Kg/S)	T (K)	$v$ (m <sup>2</sup> /s)	$\Delta P$ (Pa)
1	101740	0.206651243	295.3	1.53E-05	5.729045
2	101780	0.206651243	295.2	1.53E-05	5.729045
3	101850	0.205381419	295.1	1.53E-05	5.479956
4	101900	0.205381419	295.1	1.53E-05	5.479956
5	101890	0.206651243	294.9	1.53E-05	5.729045
Mean	101832	0.206143314	295.12	1.53E-05	5.629409
Std-Dev	69.78538529	0.000695511	0.148324	1.33E-08	0.136432

From Table 7-2 using the mean and standard deviation, the uncertainty for Re and pressure drop were calculated to be

- $Re = 70014.7434$ 
  - Error =  $\pm 393.3402$
  - Error percentage = 0.5618 %
- $\Delta P = 5.629409$ 
  - Error =  $\pm 0.1697$
  - Error Percentage = 0.0301 %

As the uncertainty of  $Re$  and  $\Delta P$  are much smaller, no analysis was needed to improve their uncertainty.

### 7.1.2 Student's t Distribution (N=5) - Varying Heat Flux

Another study was done to see if uncertainties were affected by taking different set of readings by varying the heat flux without switching off the experiment, instead of repeating the experiment one at a time, to mimic repeatability.

**Table 7-3: Measurement for Nu calculation (varying heat flux)**

Data	I (A)	$T_s$ (°C)	T-inlet (°C)	T-outlet (°C)	Nu
1	4.64	56.99	24.27	24.6	123.93
2	4.79	59.82	24.47	24.8	120.83
3	4.98	62.16	24.73	25	125.13
4	5.03	63.58	24.87	25.2	122.16
5	5.19	65.07	24.97	25.3	128.13
Mean	4.926	61.525	24.66	24.98	124.04
Std-Dev	0.214313	3.189573	0.28906	0.286356	2.818099

From table 7-3 the uncertainty for Nu was calculated using the average value and standard deviation of each parameter,

- $Nu = 123.7902$ 
  - Error =  $\pm 31.12, \pm 30.61$

- Error percentage = 25.14 %, 24.73 %

This method gives an error of 24.73-25.14% in comparison to 8.01-8.75 % using the regular method. Therefore, varying the heat flux is not the best practice to calculate uncertainty.

Instead of using the conventional method in calculating the uncertainty, Nu values of each data are calculated. Considering Nu to be a single measurement, the random uncertainty is calculated.

- Nu = 124.04
  - Error =  $\pm 3.49$
  - Error percentage = 2.71 %

The uncertainty produced by this method is less in comparison to 8.75 % using the regular method. Hence considering Nu to be a single measurement is not the best practice in calculating the uncertainty.

## 7.2 Optimized Ribs

According to the secondary objective three ribs shown in section 4.4 were compared in terms of Nu and pressure drop. A current of 5.647 A is used in all the experiments. From Figure 7-9, all three ribs have close mean Nu in low Re. But in high Re Rib 2 performs better in comparison to the other ribs, due to increase in turbulence created by this rib.

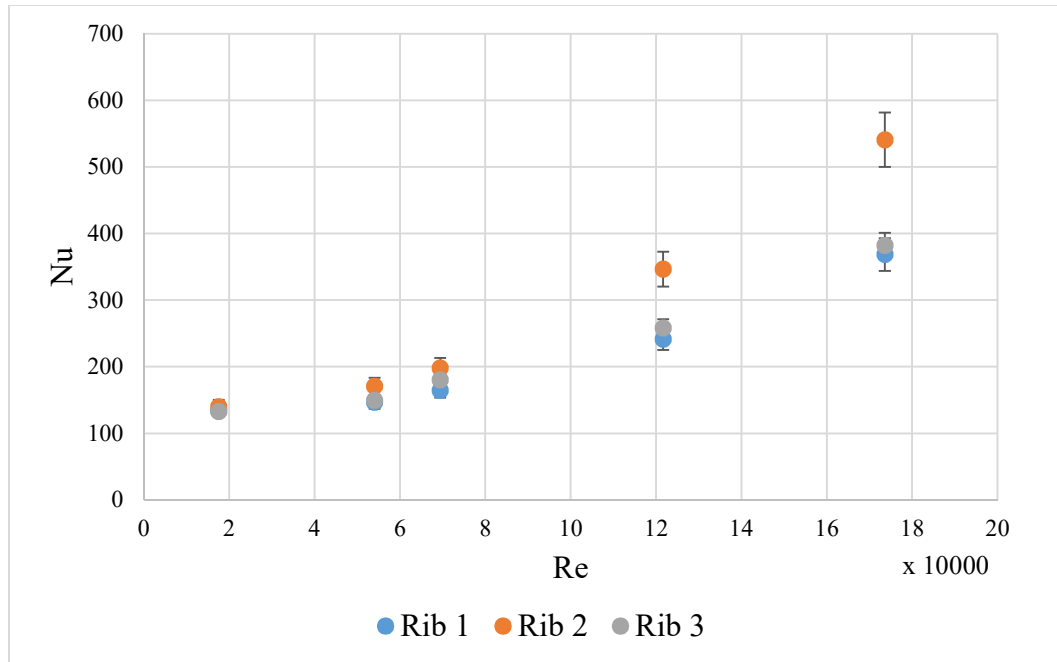


**Figure 7-9: Nu comparison**

In Figure 7-10 it is clearly seen that Rib 3 performs better in comparisons to the other ribs. Therefore, we can conclude that rib 3 performs overall better in heat transfer and pressure drop. But in literature review it was found that rib 1 performs better in comparison to the other ribs and this may be due to the difference in the setup between CFD model and experiment. In the experiment only one rib of each kind was used, but in CFD a symmetrical setup was used.

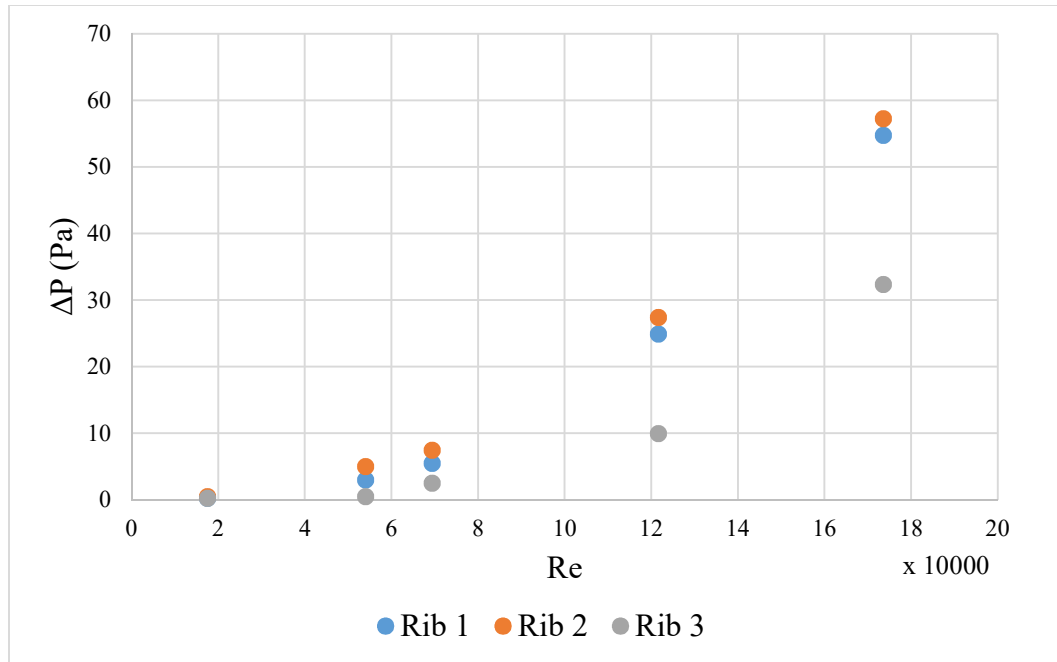


**Figure 7-10: Pressure drop comparison**

### 7.3 Pin-Fin Channel

From section 7.1 it was found that the main contributor to the uncertainty is the current measured from the VARIAC, therefore a shunt resistor (shown in Figure 7-11) was used to calculate the current, using a high precision multi-meter to record the voltage across the shunt. The shunt resistor will have low resistance and the expected voltage drop across it will be small. The results were analyzed to see whether there is an improvement in the calculated uncertainty.



**Figure 7-11: Shunt resistor**

Figure 7-12, 7-13, 7-14 show the temperature contour, Nu contour, and the spanwise Nu for Re of 25000 and heat flux of  $5600 \text{ W/m}^2$ .

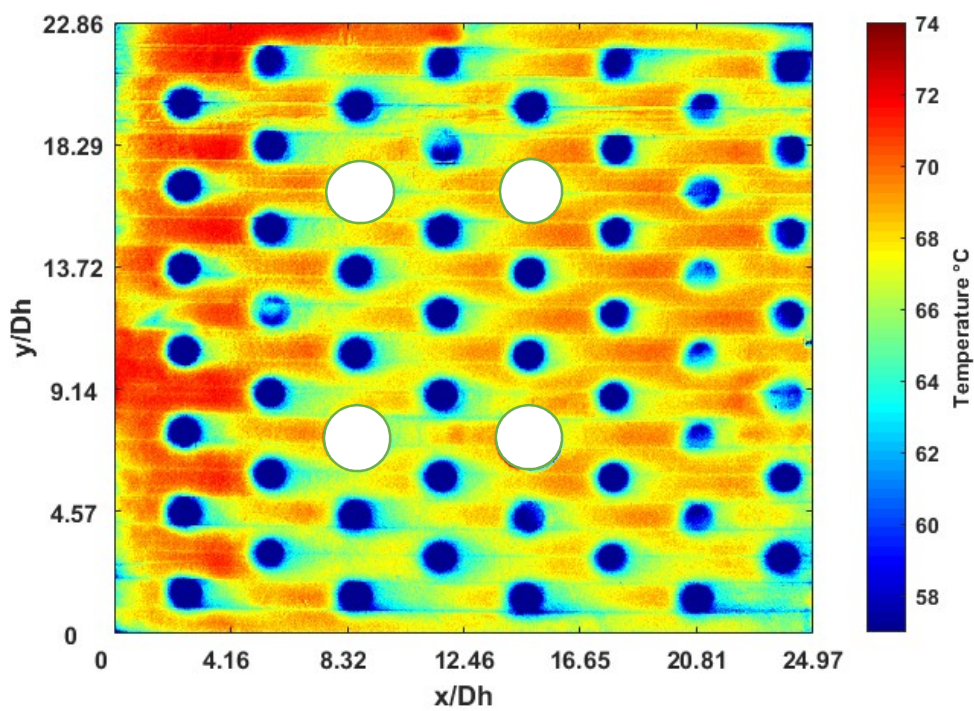


**Figure 7-12: Temperature contour – Pin fin**

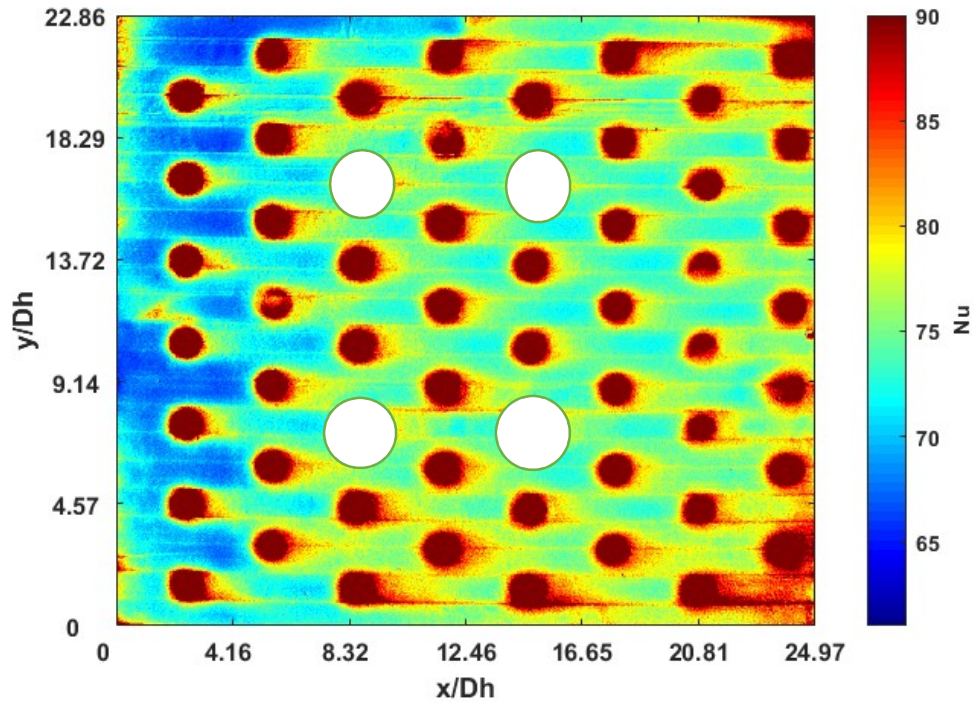


Figure 7-13: Nu contour – Pin fin

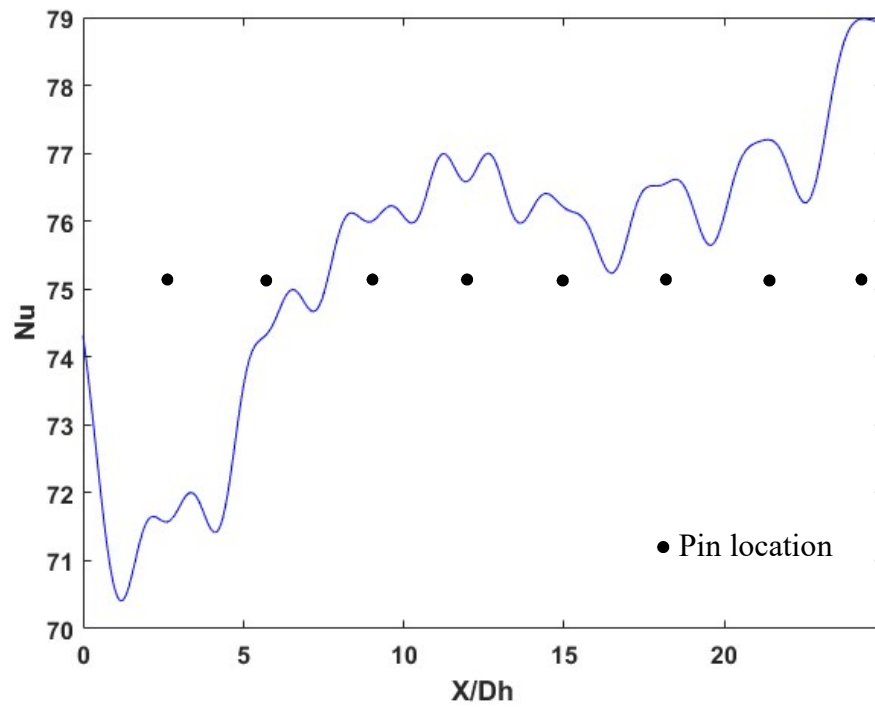


Figure 7-14: Span wise average Nu – Pin fin



As seen in Figure 6-11, four bolts are used to secure the top and the bottom acrylic plate to make the pins touch the end wall, as previous experiments revealed the end wall to warp a little by the heat supplied, which removes the contact of the pins from the end wall. The area covered by the bolts is neglected as shown in Figure 7.12 and 7.13 along with the area under the pins in post processing, to get proper span-wise average Nu. The pins were not heated for all the experiments.

The characteristic length was taken to be the pin diameter which is 0.015 m and the pressure drop was measured to be 214 Pa. From Figure 7-13 it can be observed that a horse shoe vortex is formed at front around the edge and sheds behind the pin, and a stagnation region is formed in front of the pin. These improve heat transfer rate in the respective regions, which is indicated by the two peaks before and after the pin in Figure 7-14. The shunt resistor has low resistance about 0.00375  $\Omega$ , hence current can be measured more accurately across the shunt.

### **7.3.1 Student's t Distribution (N=5) – Pin Fin Channel**

The experiment was repeated 5 times, with same Re of 25000. Between each repetition the experiment was switched off and started from the beginning for repeatability. The bias error for the digital multi-meter (Keithley 2100) is given by,

- Resolution = 0.1  $\mu\text{v}$
- Range = 100 mv
- Accuracy = +/- (0.08 of Reading + 0.05 of Range)

The remaining bias errors in measurement is same as given in section 7.1.1. The multi-meter measurement is taken in terms of milli-volt, which is later converted to current (A) in calculating the heat supplied.

**Table 7-4: Measurements for Nu calculation (Pin fin)**

Data	I (A) - VARIAC	V (mv) - Keithley	T <sub>s</sub> (°C)	T-inlet (°C)	T-outlet (°C)
1	10.57	39.621	67.06	23.2	29.5
2	10.58	39.639	67.63	23.7	30
3	10.57	39.614	66.92	23.2	29.6
4	10.61	39.773	67.80	23.6	30
5	10.62	39.823	68.19	23.8	30.1
Mean	10.59	39.694	67.519	23.5	29.84
Std-Dev	0.023452079	0.097	0.526945	0.282843	0.270185

Using the measurements from Table 7-4, the uncertainties in Nu were calculated. The Surface temperature given in Table 7-4 is the mean value obtained from post processing the TSP data image. Similarly, a minimum and a maximum temperature values (Table 7-5) were also obtained in post processing to compare with the calculated uncertainties (Table 7-6).

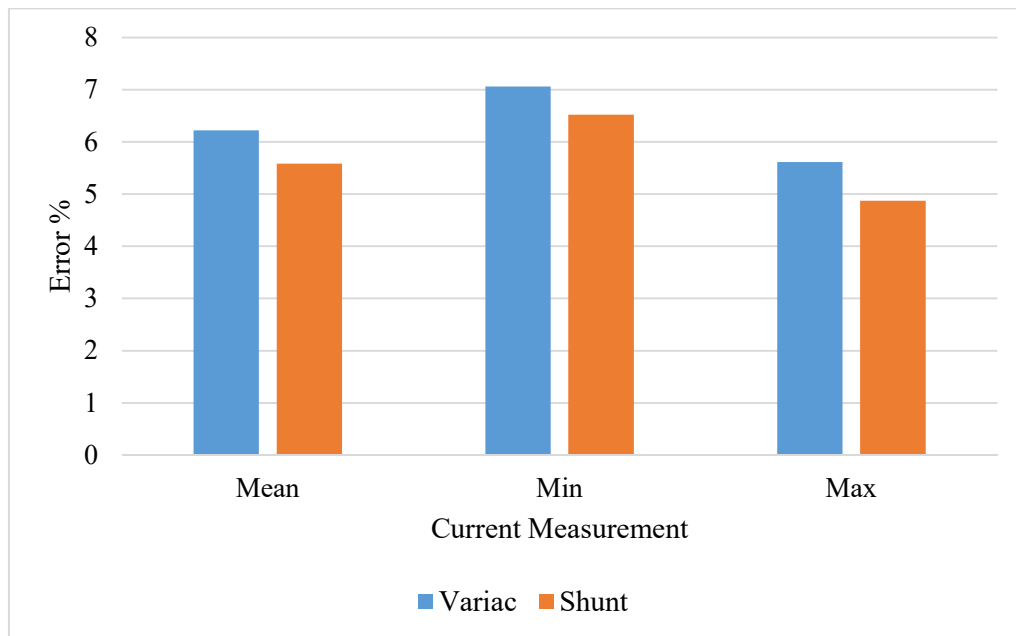
**Table 7-5: Mean, min, max temperature measurements**

Data	T <sub>s</sub> -Mean (°C)	T <sub>s</sub> -Min (°C)	T <sub>s</sub> -Max (°C)
1	67.06	63.09	73.08
2	67.63	63.67	73.37
3	66.92	61.89	72.44
4	67.80	63.25	73.46
5	68.19	63.90	73.44
Mean	67.519	63.166	73.162
Std-Dev	0.526945	0.778879	0.431048

**Table 7-6: Uncertainty results**

		Nu	Error	% Error
VARIAC	Mean	78.13	$\pm 4.86$ $\pm 4.59$	6.220 5.885
	Min	88.825	$\pm 6.27$ $\pm 6.02$	7.061 6.777
	Max	67.253	$\pm 3.78$ $\pm 3.52$	5.618 5.228
Shunt	Mean	78.05	$\pm 4.35$	5.584
	Min	88.729	$\pm 5.79$	6.525
	Max	67.179	$\pm 3.27$	4.872

From Figure 7-15, calculating the current supplied by using a shunt resistor gives less percentage error in mean, minimum and maximum Nu values, in comparison to current recorded from the digital ammeter in the VARIAC.

**Figure 7-15: Comparison of percentage of error**

In comparison to the error in Figure 7-4, the error in Figure 7-16 has reduced by 56.956 % due to improved current measurement (Figure 7-17) and the resulting improvement in the calculation of Nu.

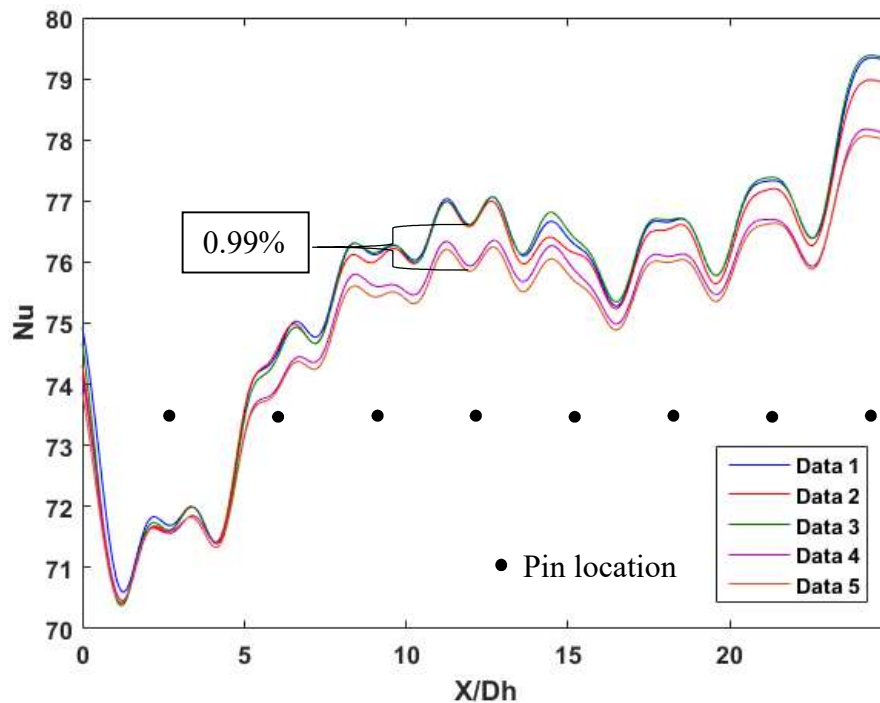


**Figure 7-16: Span-wise average Nu comparison (pin fin)**

As seen in Figure 7-17, the difference in current recorded from the ammeter in the VARIAC from the current calculated from the measured voltage across the shunt resistor using the Keithley multi-meter, leads to the improvement in Nusselt Number calculation as mentioned above.

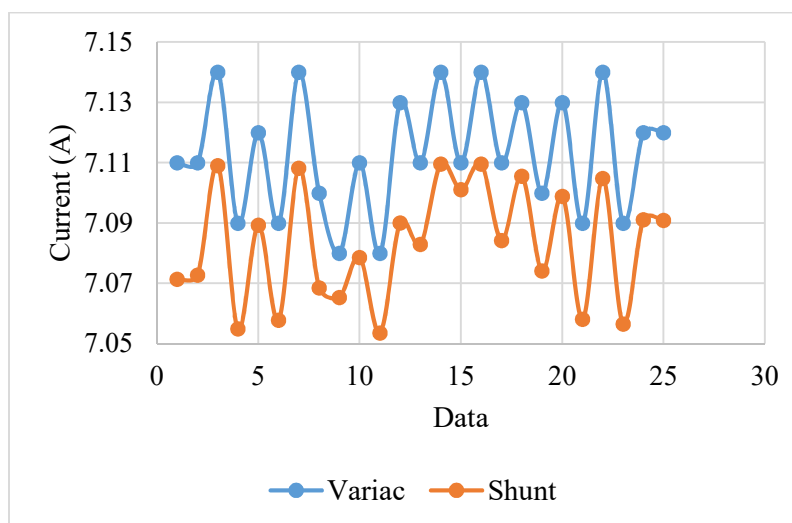


**Figure 7-17: Comparison of current**

### 7.3.2 Effect of $\Delta T$

**Table 7-7: Measurements for Nu calculation effect of  $\Delta T$**

Data	V- (mv) - Keithley	T <sub>s</sub> (°C)	T-inlet (°C)	T-outlet (°C)
1	26.585	49.07	22.7	26
2	26.545	49.22	22.4	25.8
3	26.629	48.51	21.9	25.5
4	26.621	47.77	23	26.3
5	26.591	48.36	22.7	25.3
Mean	26.5942	48.586	22.54	25.78
Std-Dev	0.033334667	0.582535	0.415933	0.396232

The uncertainty calculated using the shunt resistor in section 7.3.1 is compared from the uncertainty calculated using Table 7-7. The value of  $\Delta T$  (difference between T<sub>s</sub> and T<sub>b</sub>) obtained in section 7.3.1 is 40.85 °C and the value of  $\Delta T$  obtained from Table 7-7 is 24.44 °C. The calculated values are,

- Nu = 56.031
- Error =  $\pm 5.3379$
- Percentage Error = 9.5267 %

From Figure 7-18, it is found that by increase in  $\Delta T$  the error decreases. Hence having a high surface temperature will result in less uncertainty but on the other hand entails the risk of damaging the acrylic end wall.

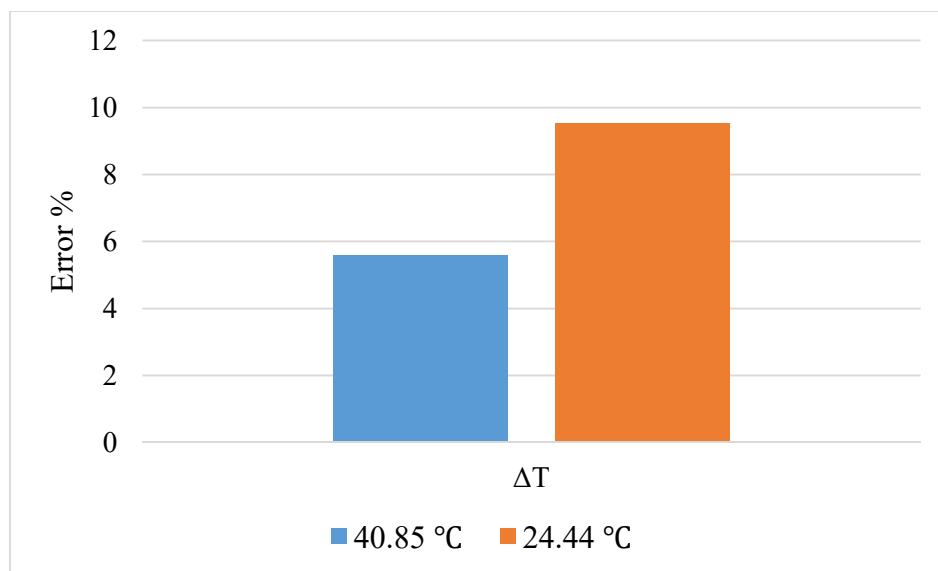


**Figure 7-18: Comparison of % error with respect to  $\Delta T$**

### 7.3.3 Student's t Distribution Vs Normal Distribution

Uncertainty using a Student's t distribution of 5 samples is compared to the calculated uncertainty using 25 samples representing a normal distribution. Initially 30 samples were aimed to be obtained as discussed in the introduction to the uncertainty but the connections between the strips were lost after the 25<sup>th</sup> repetition.

**Table 7-8: Measurements for Nu calculation using different sample size**

		V-(mv)- Keithley	TS (°C)	T-inlet (°C)	T-outlet (°C)
N = 25	Mean	26.5632	48.427	22.624	25.956
	Std-Dev	0.072514	0.833803	0.615955	0.610382
N = 5	Mean	26.5942	48.587	22.54	25.78
	Std-Dev	0.033335	0.582535	0.415933	0.396232

**Table 7-9: Uncertainty results for different sample size**

	Nu	Error	Error %
N = 5	56.79	± 5.338	9.53
N = 25	56.64	± 5.187	9.74

Using the measurements in Table 7-8 the uncertainty was calculated for different sample size as seen in Table 7-9. This gives about 2.15 % difference, between the % error in uncertainties. But 2.15% is not significantly high, therefore repeating the experiment less number of times is significant enough to perform the uncertainty calculation. As it has been found that repeating the experiment more number of times has a considerable impact on the apparatus.

The 5 sample size were taken random from within 25 samples. For further comparison, samples of first 5 and last 5 from 25 samples were taken. The uncertainties were calculated and tabulated in Table 7-11.

**Table 7-10 Measurements for Nu calculation**

		V-(mv)- Keithley	TS (°C)	T-inlet (°C)	T-outlet (°C)
N = 5 (1-5)	Mean	26.5482	49.240	23.22	26.52
	Std-Dev	0.07694	0.60253	0.38340	0.38340
N = 5 (20-25)	Mean	26.5512	48.951	22.72	25.74
	Std-Dev	0.08147	0.54282	0.08366	0.56833

**Table 7-11 Uncertainty results**

	Nu	Error	Error %
N = 5 (1-5)	55.82	± 1.93	9.61
N = 5 (20-25)	55.04	± 1.86	9.39

Using the measurements in Table 7-10 the uncertainty was calculated and tabulated in Table 7-11. In comparing the results from Table 7-9 and 7-11, it is seen that the difference between uncertainties using less number and large number of samples does not produce significant difference between them. Using first 5 samples (1-5) it gives about 1.3% difference in percentage error and using last 5 samples (20-25) it gives about 3.5%

difference in percentage error. The uncertainty calculated using 25 sample size gives a percentage error of 9.74 %, this is marginally high in comparison, since TSP degrades over time and usage, explained in section 7.4.

From Figure 7-19, the PDF of student's t distribution for a sample size of 25 is much closer to the PDF of normal distribution, hence the comparison between sample size of 5 and 25 is valid.

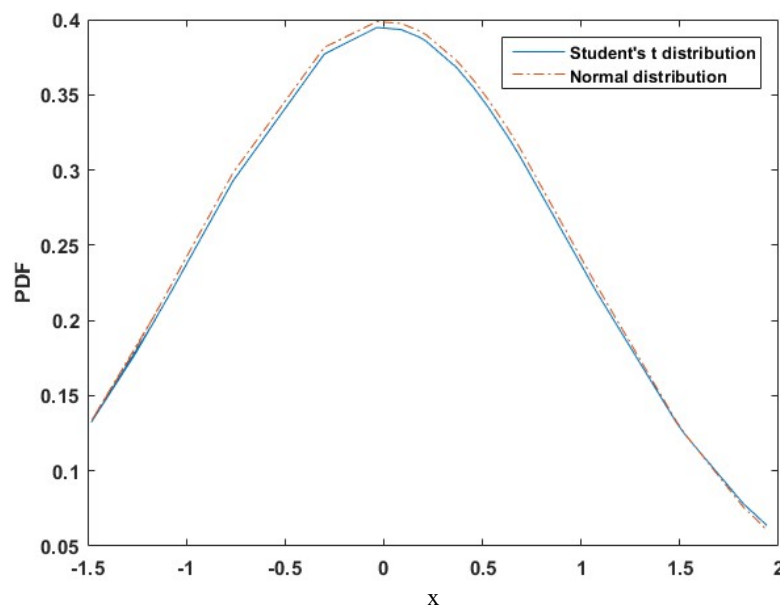


**Figure 7-19: Comparison of PDF**

#### **7.3.4 Accuracy and Precision**

From Figure 7-20 it is seen that the values of Nu obtained from post processing are not accurate with respect to the calculated mean value obtained in uncertainty calculation using the measurements from Table 7-4.



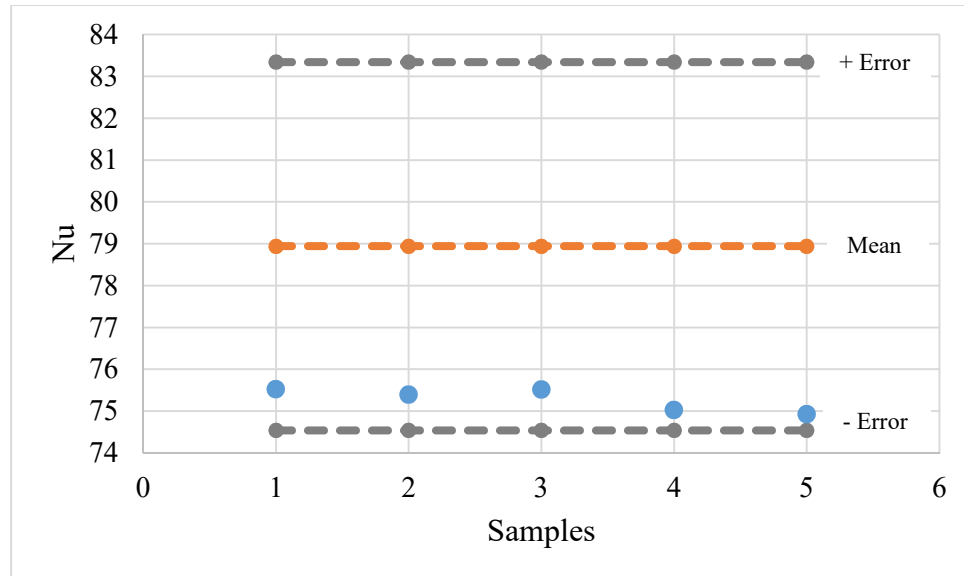


**Figure 7-20: Accuracy and Precision**

It was found out that the  $T_{outlet}$  temperature obtained from the thermocouple had a higher value in comparison to the  $T_{outlet}$  temperature obtained using the energy balance equation.

$$T_{outlet} = T_{inlet} + \frac{q}{\dot{m}C_p}$$

Therefore, instead of using the  $T_{outlet}$  reading from the thermocouple, Nu was calculated using the above mentioned equation in calculating the uncertainty. The mean value with its errors were obtained.

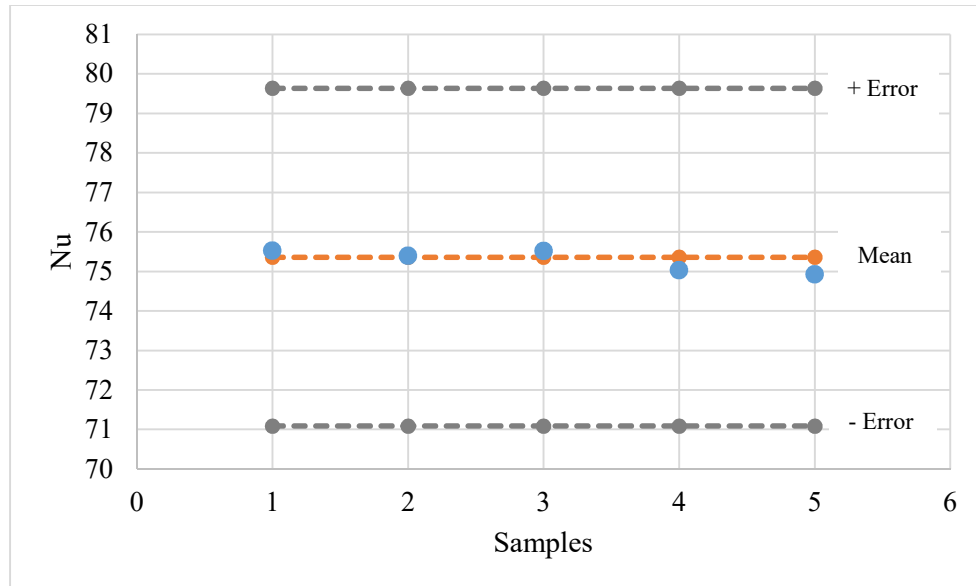


**Figure 7-21: Accuracy and Precision - Corrected**

From Figure 7-21, it is seen that from making the correction the values of Nu obtained from post processing are accurate and precise with respect to the calculated mean Nu in uncertainty. The values of mass flow rate and  $C_p$  are kept constant when implementing the energy balance equation in uncertainty calculation. Only the bias and precision error of  $T_{inlet}$  and heat supplied were propagated. The calculated uncertainty came out to be,

- $Nu = 75.36$
- $Error = \pm 4.2748$
- $Percentage\ Error = 5.6725\ %$

The values obtained have similar errors in comparison to the errors obtained before making the correction. And a slight change in  $\Delta T$  from  $40.85\ ^\circ C$  to  $42.50\ ^\circ C$ . The higher temperature value obtained from the thermocouple may be due to its positioning in the experimental apparatus, which led to reading from a particular hot streak of air. Therefore,

a recommendation from this finding is to have an array of thermocouples in the span-wise direction at the exit and average out the measurements to get a proper value.

#### 7.4 Degradation of TSP

The intensity (the measure of photons emitted, which are then captured by the CMOS sensor) of the TSP paint was recorded from the reference image taken over 3 sec exposure time for each measurement. Four reference and data images are taken for post processing to average out to remove smaller deviations in intensity. From Figure 7-22 it is found that the intensity of TSP degrades gradually with increase in usage of TSP.

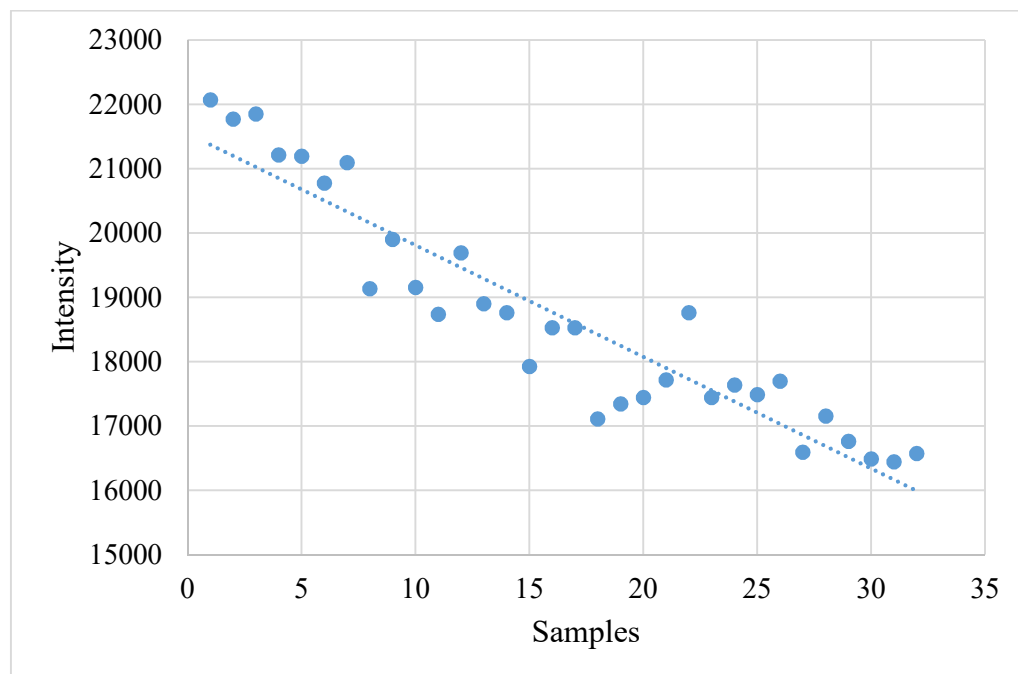


**Figure 7-22: Degradation of TSP**

Therefore, a suggestion from this finding which correlates to the calculating the uncertainty using large number of samples is that it leads to degradation of TSP. This

supports the calculation of uncertainty using less number samples, which preserves the TSP for a longer duration, which can be used to take subsequent measurements.

## 8. Conclusion

This study was concerned with the detailed analysis of uncertainty in heat transfer experiments. When the uncertainty was calculated by using student's t distribution of 5 samples, it was found that current reading taken from the ammeter in the VARIAC gave a high contribution to the uncertainty. Therefore, a different way to measure the current was implemented. By this method a shunt resistor was used to measure voltage reading across it using a precision multi-meter. It was later converted into current. The shunt resistor gave out a different current measurement since the resistance offered from the shunt was small and multi-meter (keithley) had high accuracy. This implementation brought down the percentage error from an average (mean, minimum, maximum Nu) of 6.13% to 5.66%. Another major contributor to the uncertainty was the  $\Delta T$  (difference between the surface to bulk temperature) which is used to calculate the heat transfer coefficient. Higher the  $\Delta T$ , less the uncertainty. But for a higher  $\Delta T$  the surface temperature has to be increased, which degrades the TSP faster, expands the strips and increases the possibility of short circuiting. Hence it was also the reason to go for calculating the uncertainty using less samples. It is proved that the uncertainty calculated using 5 sample and using 25 sample had similar results with 2.15 % difference in percentage error. Repeating the experiment more number of times just for uncertainty will consume a lot of time and resource, considering the fact that heat transfer experiments takes a longer time to attain steady state (average of 2 hours is needed for a single reading). During this study it was found that the thermocouple used to obtain the outlet temperature gives a higher reading in comparison to the value obtained from using an energy balance equation. Therefore, it is recommended that an array of thermocouples be used in the span wise direction at the outlet, such that the data obtained

can be averaged out to get a proper reading. Using the TSP, a number of times leads to its degradation, hence calculating uncertainty using large number of samples is not recommended.

A secondary study was done to compare three modified ribs. It is found out that rib 3 performs overall well in terms of heat transfer and pressure drop. This finding was different for the literature, since in the literature a symmetrical setup of each rib was used in the CFD analysis and this may have produced different results in comparison to the results obtained using a single rib in the experiment. Further CFD analysis is needed to support these findings.

## REFERENCES

- Ames, F. E., & Dvorak, L. A. (2006). Turbulent transport in pin fin arrays: experimental data and predictions. *Journal of turbomachinery*, 128(1), 71-81.
- ASME PTC 19.1 (2005). "Test Uncertainty". American Society of Mechanical Engineers.
- Bell, James, Schairer, E., Hand, L., Mehta, R. (2001). "Surface Pressure Measurements Using Luminescent Coatings". *Journal of Fluid Mechanics*, 33, pp 155-206.
- Bernard L. Koff (2004). "Gas Turbine Technology Evolution: A Designer's Perspective". Turbo Vision, Inc., Palm Beach Gardens, Florida.
- Bhushan Upalkar (2015). An Investigation of Cooling Configurations in Gas Turbine Engines using Jet Impingement, Thesis, Embry Riddle Aeronautical University.
- Catherine Forbes, Merran Evans, Nicholas Hastings, Brian Peacock (2011). *Statistical Distributions*, Fourth Edition.
- Chyu, M. K., Hsing, Y. C., Shih, T. P., & Natarajan, V. (1999). Heat transfer contributions of pins and endwall in pin-fin arrays: effects of thermal boundary condition modeling. *Journal of Turbomachinery*, 121(2), 257-263.
- Clifford, R.J. (1985). "Rotating Heat Transfer Investigations on a Multipass Cooling Geometry." AGARD CP 390.
- Downs, J. P., & Landis, K. K. (2009). *Turbine Cooling Systems Design: Past, Present and Future. Volume 3: Heat Transfer, Parts A and B.*
- Han, J. C., Dutta, S., & Ekkad, S. (2012). *Gas turbine heat transfer and cooling technology.* CRC Press.
- Han, J. C. (2004). Recent studies in turbine blade cooling. *International Journal of Rotating Machinery*, 10(6), 443-457.
- Han, J. C., J. S. Park, and C. K. Lei. "Heat Transfer Enhancement in Channels with Turbulence Promoters." *Journal of Engineering for Gas Turbines and Power* 107 (1985): 628. Print.
- Holman, J.P., *Heat Transfer*, Tenth Edition.
- Iacovides, H, Launder, B.E. (2006). "Internal blade cooling: The Cinderella of computational and experimental fluid dynamics research in gas turbines". The University of Manchester, Manchester, UK.

- Isheeta Ranade, Jaime Gutierrez, Eloy Guillen, Yash Mehta, Mark Ricklick (2016). "Development of Novel Internal Cooling Geometry for Gas Turbine Blades". Embry-Riddle Aeronautical University, USA.
- ISSI, Innovative Scientific Solutions, Temperature Sensitive Paint, <http://www.psp-tsp.com/index.php?id=123>.
- ISSI, Innovative Scientific Solutions, High-intensity light sources, <http://www.psp-tsp.com/index.php?id=213>.
- Kline, S.J., McClintock, F. A. (1953). "Describing the Uncertainties in single sample experiments". Mech. Eng., 3-8.
- Keithley Instruments, Inc. Keithley 61/2 Resolution Digital Multimeter Specifications, [http://www.tek.com/sites/tek.com/files/media/document/resources/SPEC-2100C\\_Sep2011\\_Customer.pdf](http://www.tek.com/sites/tek.com/files/media/document/resources/SPEC-2100C_Sep2011_Customer.pdf)
- Lavagnoli, Sergio, Maesschalck, Cis De, Paniagua, Guillermo (2015). Uncertainty Analysis of Adiabatic Wall Temperature Measurements in Turbine Experiments. Applied Thermal Engineering 82 170-181.
- Liu, T., Campbell, B., Sullivan, J. (1995). "Accuracy of TSP for heat transfer measurements". AIAA 95-2042.
- Liu, Quan, Kapat, J. (May 2006). "Study of Heat Transfer Characteristics of Impinging Air Jet Using Pressure and Temperature Sensitive Luminescent Paint". UCF Dissertation.
- McQuillan, F.J., Culham, J.R. and Yovanovich, M.M. (1984). Properties of Dry Air at 1 Atmosphere, University of Waterloo, Ontario.
- Metzger, D. E., & Haley, S. W. (1982, April). Heat transfer experiments and flow visualization for arrays of short pin fins. In ASME 1982 International Gas Turbine Conference and Exhibit (pp. V004T09A007-V004T09A007). American Society of Mechanical Engineers.
- Moffat, Robert J. (1988). "Describing the Uncertainties in Experimental Results". Stanford University, Stanford, California.
- Mohammad Ahsanullah, B.M. Golam Kibria, Mohammad Shakil (2014). Normal and Student's t Distribution and their Applications.
- Royce Fernandes (2016). Investigation of Pin Fin Cooling Channels for Applications in Gas Turbines. Master Thesis, Embry Riddle Aeronautical University.



- OMEGA, Revised Thermocouple Reference Tables for Type T Thermocouple, <http://www.omega.com/temperature/Z/pdf/z207.pdf>.
- Wen Yao, Xiaoqian Chen, Wencai Luo, Michel van Tooren, Jian Guo (2011). "Review of uncertainty-based multidisciplinary design optimization methods for aerospace vehicles". *Progress in Aerospace Sciences* 47, 450-479.
- Yash T. Mehta (2015). *Experimental and Computational Investigation of Ribbed Channels for Gas Turbine Thermal Management*. Master Thesis, Embry Riddle Aeronautical University.
- Yogesh Pai (2016-on progress). *Extended Surface Heat Transfer Co-efficient Via End-Wall Temperature Measurements*. Master Thesis, Embry Riddle Aeronautical University.
- Zuckerman, N., & Lior, N. (2006). Jet Impingement Heat Transfer: Physics, Correlations, and Numerical Modeling. *Advances in Heat Transfer*, 565-631, 2006.
- Zuckerman N., Lior N. (2005). "Impingement Heat Transfer: Co-relations and Numerical Modeling". *International Journal of Heat Transfer*.

## APPENDIX

**A. Data Reduction****Power Supplied:**

The power (q) is supplied to the heater strips through a VARIAC having a digital ammeter in it. The systematic and random uncertainty of the current given is calculated by

$$B_I = \sqrt{e_1^2 + e_2^2 \dots \dots e_n^2}$$

$$b_I = \frac{B_I}{t_{95}}$$

$$S_I = \frac{\sigma_I}{\sqrt{N}}$$

The resistance of the heater strips is taken to be constant. Therefore, the systematic and random uncertainty of the power supplied to the heater strips is calculated by

$$b_q = \sqrt{\left(\frac{\partial q}{\partial I} * b_I\right)^2}$$

$$S_q = \sqrt{\left(\frac{\partial q}{\partial I} * S_I\right)^2}$$

**Temperature Difference ( $\Delta T$ ):**

The temperature difference is given by the difference between the surface and the bulb temperature. In which the average surface temperature ( $T_s$ ) is obtained from post processing the raw TSP data using a MATLAB code. The systematic error for the surface temperature is assumed. Therefore, the systematic and random uncertainty is given by,

$$B_{T_s} = \sqrt{e_1^2}$$

$$b_{T_s} = \frac{B_{T_s}}{t_{95}}$$

$$S_{T_s} = \frac{\sigma_{T_s}}{\sqrt{N}}$$

The bulk temperature ( $T_b$ ) is obtained from the energy balance equation as explained in Figure 3-2, but since mean values are used in calculating the uncertainty, the bulk temperature is taken as the average between inlet and outlet temperature. And its systematic and random uncertainty is calculated by,

$$B_{T_{inlet}} = \sqrt{e_1^2 + e_2^2 \dots \dots e_n^2}$$

$$b_{T_{inlet}} = \frac{B_{T_{inlet}}}{t_{95}}$$

$$S_{T_{inlet}} = \frac{\sigma_{T_{inlet}}}{\sqrt{N}}$$

$$B_{T_{outlet}} = \sqrt{e_1^2 + e_2^2 \dots \dots e_n^2}$$

$$b_{T_{outlet}} = \frac{B_{T_{outlet}}}{t_{95}}$$

$$S_{T_{outlet}} = \frac{\sigma_{T_{outlet}}}{\sqrt{N}}$$

$$b_{T_b} = \sqrt{\left(\frac{\partial T_b}{\partial T_{inlet}} * b_{T_{inlet}}\right)^2 + \left(\frac{\partial T_b}{\partial T_{outlet}} * b_{T_{outlet}}\right)^2}$$

$$S_{T_b} = \sqrt{\left(\frac{\partial T_b}{\partial T_{inlet}} * S_{T_{inlet}}\right)^2 + \left(\frac{\partial T_b}{\partial T_{outlet}} * S_{T_{outlet}}\right)^2}$$

Having calculated the systematic and random uncertainty for both surface and bulk temperature, the uncertainty for the temperature difference is given by,

$$b_{\Delta T} = \sqrt{\left(\frac{\partial \Delta T}{\partial T_b} * b_{T_b}\right)^2 + \left(\frac{\partial \Delta T}{\partial T_s} * b_{T_s}\right)^2}$$

$$S_{\Delta T} = \sqrt{\left(\frac{\partial \Delta T}{\partial T_b} * S_{T_b}\right)^2 + \left(\frac{\partial \Delta T}{\partial T_s} * S_{T_s}\right)^2}$$

### Heat Transfer Coefficient:

The surface areas of the strips ( $A_1$ ) are taken to be constant, hence there will be no error from its part. The systematic and random uncertainty for the power supplied and the temperature difference are calculated in the previous steps. Hence the uncertainty by the heat transfer coefficient is given by,

$$b_h = \sqrt{\left(\frac{\partial h}{\partial q} * b_q\right)^2 + \left(\frac{\partial h}{\partial \Delta T} * b_{\Delta T}\right)^2}$$

$$S_h = \sqrt{\left(\frac{\partial h}{\partial q} * S_q\right)^2 + \left(\frac{\partial h}{\partial \Delta T} * S_{\Delta T}\right)^2}$$

### Reynolds Number:

$$b_\rho = \sqrt{\left(\frac{\partial \rho}{\partial P} * b_P\right)^2 + \left(\frac{\partial \rho}{\partial T} * b_T\right)^2}$$

$$S_\rho = \sqrt{\left(\frac{\partial \rho}{\partial P} * S_P\right)^2 + \left(\frac{\partial \rho}{\partial T} * S_T\right)^2}$$

$$b_\mu = \sqrt{\left(\frac{\partial \mu}{\partial \rho} * b_\rho\right)^2 + \left(\frac{\partial \mu}{\partial v} * b_v\right)^2}$$

$$S_\mu = \sqrt{\left(\frac{\partial \mu}{\partial \rho} * S_\rho\right)^2 + \left(\frac{\partial \mu}{\partial v} * S_v\right)^2}$$

$$b_{Re} = \sqrt{\left(\frac{\partial R}{\partial \dot{m}} * b_{\dot{m}}\right)^2 + \left(\frac{\partial R}{\partial \mu} * b_\mu\right)^2}$$

$$S_{Re} = \sqrt{\left(\frac{\partial Re}{\partial \dot{m}} * S_{\dot{m}}\right)^2 + \left(\frac{\partial R}{\partial \mu} * S_{\mu}\right)^2}$$

The final uncertainty with 95 % confidence is calculated by,

$$u_{Re} = \sqrt{b_{Re}^2 + S_{Re}^2}$$

$$U_{Re} = t_{95} * u_{Re}$$